ASIA TURBOMACHINERY & PUMP SYMPOSIUM

HIGH SPEED BALANCING: API ACCEPTANCE CRITERIA, PEDESTAL DYNAMICS, AND UNBALANCE RESPONSE

Brian Hantz
Mechanical Engineer
Elliott Group
Jeannette, Pennsylvania

Qingyu Wang
Mechanical Engineer
Elliott Group
Jeannette, Pennsylvania

Brian C. Pettinato
Mechanical Engineer
Elliott Group
Jeannette, Pennsylvania

Brian Hantz is a Mechanical Engineer at Elliott Group in Jeannette, Pennsylvania. He has been with Elliott Group since 2014. His areas of expertise include vibration and modal testing. He received his B.S. in Aerospace Engineering from Penn State University in 2012. Prior to joining Elliott Group, he worked as a dynamics engineer at Sikorsky Aircraft Corporation.

Qingyu Wang is a Mechanical Engineer at Elliott Group in Jeannette, Pennsylvania. He has been with Elliott Group since 2005. His areas of expertise include lateral and torsional rotordynamics. He received his B.S. and M.S. both in Mechanical Engineering from Tsinghua University, 1997 and 2000 respectively. He received his Ph.D in Mechanical Engineering from the University of Virginia, 2008. He serves on the API 684 rotordynamics task force, and is a member of ASME.

Brian Pettinato is Manager of Aero and Structural Dynamics at Elliott Group in Jeannette, Pennsylvania. He has been with Elliott Group since 1995. His primary area of expertise is machinery dynamics. Prior to joining Elliott Group, he worked as a project engineer for CentriMarc. Mr. Pettinato received his B.S. (1989) and M.S. (1992) Mechanical Engineering degrees from the University of Virginia. He has coauthored over twenty technical papers and holds three U.S. patents. Mr. Pettinato is a fellow member of ASME, a member of STLE, and a registered Professional Engineer in the State of Pennsylvania. He serves on the Turbomachinery Advisory Committee of Texas A&M and on the API 684 rotordynamics task force.

ABSTRACT

Acceptance criteria for high-speed balancing of turbomachinery are specified in API standards based on either pedestal velocity or shaft displacement, and these are discussed in detail. Pedestal velocities are measured using velocimeters located at each pedestal whereas shaft displacements are measured using eddy-current probes adjacent to each bearing.

In addition to performing balancing, the measured displacements can also be used for verification of the unbalance response analysis. Since the pedestals are relatively soft, their dynamics need to be considered in the analysis. In this paper, multiple modal tests are conducted on 3 different pedestals: DH4, DH7, and DH70. The FRFs are parameterized to be used in a rotordynamic model. Different torques on the pedestal bolts are used to study the effect on the measured FRFs. The added-mass method is applied to DH7 pedestals with a 100 kg plug in the pedestal bore. The calculated modal mass and stiffness are compared to values identified from the measured FRFs. Unbalance verification of some shop orders is compared to the predictions with different ways of characterizing the pedestal dynamics: rigid, mass and stiffness, and the FRFs. Minor improvements are observed using the measured data comparing to the original

models and further areas of improvement are identified. The effect of vacuum on the unbalance response is also studied.

INTRODUCTION

High speed balancing, also known as operating or at-speed balancing, is often recommended for machines operating above their first critical speed. The rotor is supported on bearings which are mounted on pedestals. The pedestals must be relatively flexible to allow sufficient response to rotor unbalance. The high-speed balance acceptance criteria is dependent on the API standard and edition. One set of criteria is provided in API 612 7th edition in which the pedestal velocity is based on the pedestal stiffness. Accurate pedestal stiffness is necessary to meet the intent of the criteria.

Aside from performing balancing, a high-speed balance facility can also be used for unbalance response verification. In this case, it would be ideal to have the support (bearings and pedestals) the same as the field conditions; however, there are always differences between the support stiffness of the balancing facility, the test floor and the site. Even between different balancing facilities, there could be large differences.

As an example, *Figure 1* shows the Bode plot from Balancing Facility 1 (shut-down), and *Figure 2* shows the Bode plot of the same rotor from Balancing Facility 2 (both startup and shut-down). The rotor was balanced in Facility 1 and then shipped to Facility 2. At Facility 2, there was no balancing done, i.e. no changes made to the rotor. One facility has shop pressure-dam journal bearings and the other one has tilting-pad journal bearings.

From this example, it can be seen that both the magnitude and the locations of the peaks are different. Note that the format and scale are different. Since there is no change of the rotor, the difference has to come from the support system (bearings, pedestals and foundation), and pedestal dynamics has to be considered as a major contributor to the difference.

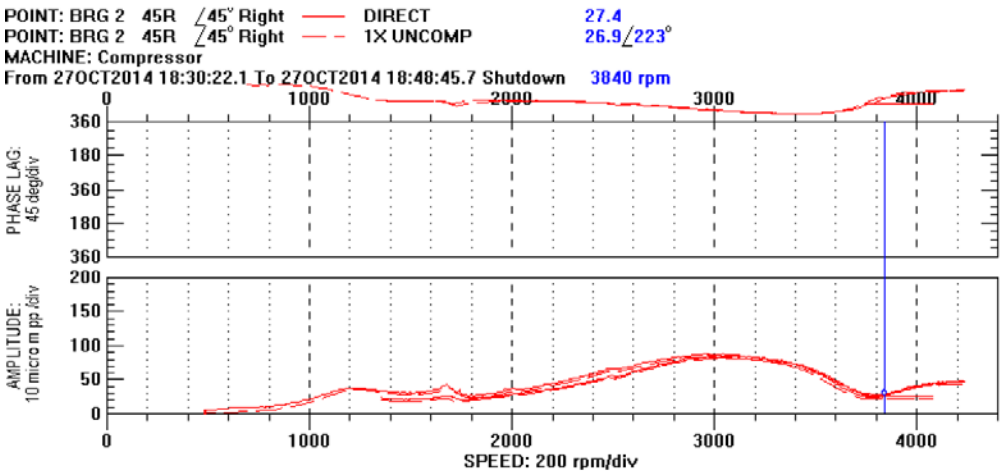

Figure 1: Bode plot from Balancing Facility 1

Note that in both figures, there seem to be two critical speeds, but the rotordynamics analysis (assuming rigid structural support behind the bearings) shows only one. There are sometime concerns regarding the second critical speed, because by design (for the field condition) it should not appear. So in those cases where the second critical speed does appear, a proper explanation is required, which is best provided by an accurate prediction. This requires an accurate pedestal model. The stiffness of the pedestal will lower the effective support stiffness. This softening of the support will decrease the frequency of the mode and place it in the operating speed range. To analyze the impact of the support stiffness on the critical speed location, accurate characterization of the pedestal dynamics is needed.

There are different ways to characterize the pedestal dynamics. A simple way is to use mass and stiffness. Usually the original pedestal manufacturer (Vendor) will provide the values, and these values are used in the balancing criteria and rotordynamic analysis. Another way is to use Frequency Response Functions (FRFs). There are numerous papers presenting the rotordynamic analysis with pedestal/support FRFs, such as Nicholas et al. (1986), Stephenson and Rouch (1992) or Vazquez et al. (2001). There are also reports of the pedestal FRFs in the Balancing Facility being measured, such as Zhou (2013). However, to the authors' knowledge, there is no publication of the FRFs from Balancing Facility being used in the rotordynamic analysis. It appears that using the pedestal FRFs would improve the rotordynamics predictions, so the authors initiated a campaign of acquiring accurate FRFs for all the pedestals, in hope of verifying the Vendor provided data and improving the predictions.

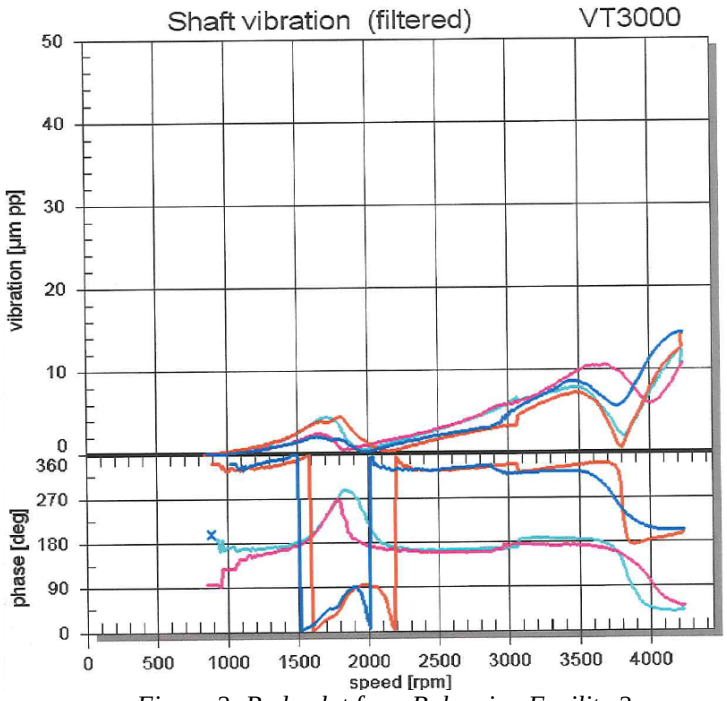

Figure 2: Bode plot from Balancing Facility 2

API BALANCING ACCEPTANCE CRITERIA

Summary of Balancing Criteria

Table 1 summarizes the high-speed balancing criteria from the API standards reviewed. Note that the table does not distinguish between "shall" or "if specified".

Table 1. API Balancing Criteria Summary

			Acceptance Criteria	
API No.	Application	Edition	High Speed	Low Speed
API 611	General Purpose Steam Turbines	5th (2008)	MA	API
API 612	Special-Purpose Steam Turbines	6th (2005)	V1	API
		7th (2014)	V1, V2, D1	
API 613	Special Purpose Gear	5th (2003)	None	API
API 616	Gas Turbines	5th (2011)	V3	API
API 617	Axial and Centrifugal Compressors and Expander-compressors	7th (2002)	V1	API
		8th (2014)	MA	
API 672	Packaged, Integrally Geared Centrifugal Air Compressors	4th (2004)	OEM	OEM
API 684	Rotordynamics Tutorial	2nd (2005)	V2	API
API 687	Rotor Repair	1st (2001)	V1	API

The abbreviations are explained as follows.

API – the maximum allowable low speed residual unbalance is specified as

In SI units:

$$U = 6350\frac{W}{N} \qquad (1)$$

In USCS units:

$$U = 4\frac{W}{N} \qquad (2)$$

where

U is the residual unbalance in g-mm (oz-in)
W is the bearing static load in kgf (lbf)
N is the maximum continuous speed in rpm

D1 – the maximum allowable shaft vibration (1X filtered and runout compensated) shall not exceed 25.4 μm peak-to-peak at any response or 12.7 μm peak-to-peak over operating speed range for probes near the bearings.

MA – mutually agreed

OEM – Manufacturer's standard balancing procedure

V1 – For all speeds at or less than 3000 rpm, the pedestal vibration shall not exceed 2.5 mm/s RMS. For speeds above 3000 rpm, the pedestal vibration shall not exceed the calculated value of (7400/*N*) mm/s or 1 mm/s RMS, whichever is the greater, where *N* is the maximum continuous speed in rpm. The criterion applies to the major axis velocity.

V2 – velocity calculated such that the maximum allowable unbalance force at any journal at maximum continuous speed shall not exceed 10 percent of the static loading of that journal.

V3 – the acceptance criterion, only used in API 616, 5th edition, is a combination of residual unbalance and pedestal vibration.

Discussion

In the early API standards, balancing was not a major part, and there were no criteria. Later on, low speed balancing criteria were added for most standards, but high speed balancing criteria only existed in certain standards. For certain types of machines, such as motors, gears, or couplings, the operating speed is in general below the first critical speed, and no high speed balance required.

The low speed criteria had always been a form of unbalance amount with some variations. In current standards, Equation (1) for g-mm or (2) for oz-in is predominantly used. ISO standards use Grade, which limits the velocity of the cg (center of gravity) of the rotor, and they are essentially the same as the API standards: the 6350*W*/*N* API standard is equivalent to ISO Grade 0.7 (API 684, 2nd edition, Paragraph 5.2.7). Note that the limit of the unbalance amount (or eccentricity of cg) has the assumption that the rotor can be simplified as a single mass.

For high speed balancing, since the rotor cannot be simplified as a single mass, limiting the unbalance amount cannot be used directly. An alternative, the V2 method (appeared first in API 617 4th edition) is to limit the force induced by the unbalance. The 10% of the static weight was suggested by Jackson (1979). There are some variations of the format, such as API 612, 7th edition, API 616 2nd edition and API 684 2nd edition, but essentially they are all the same as the V2 method.

The V1 method for high speed balancing is only related to the operating speed, and it could be largely different compared to the V2 method. With 723 shop orders from the authors' company, the relationship between V1 and V2 is shown as *Figure 3*, where the red line is the V1 method, and all the dots are calculated based on V2 method (0.2 'g', i.e. 10% static load per pedestal) using Maximum Continuous Speed (MCS), rotor weight and pedestal stiffness. The stiffness values used are Vendor provided: 560 N/μm for DH4 and 1,334 N/μm for DH7.

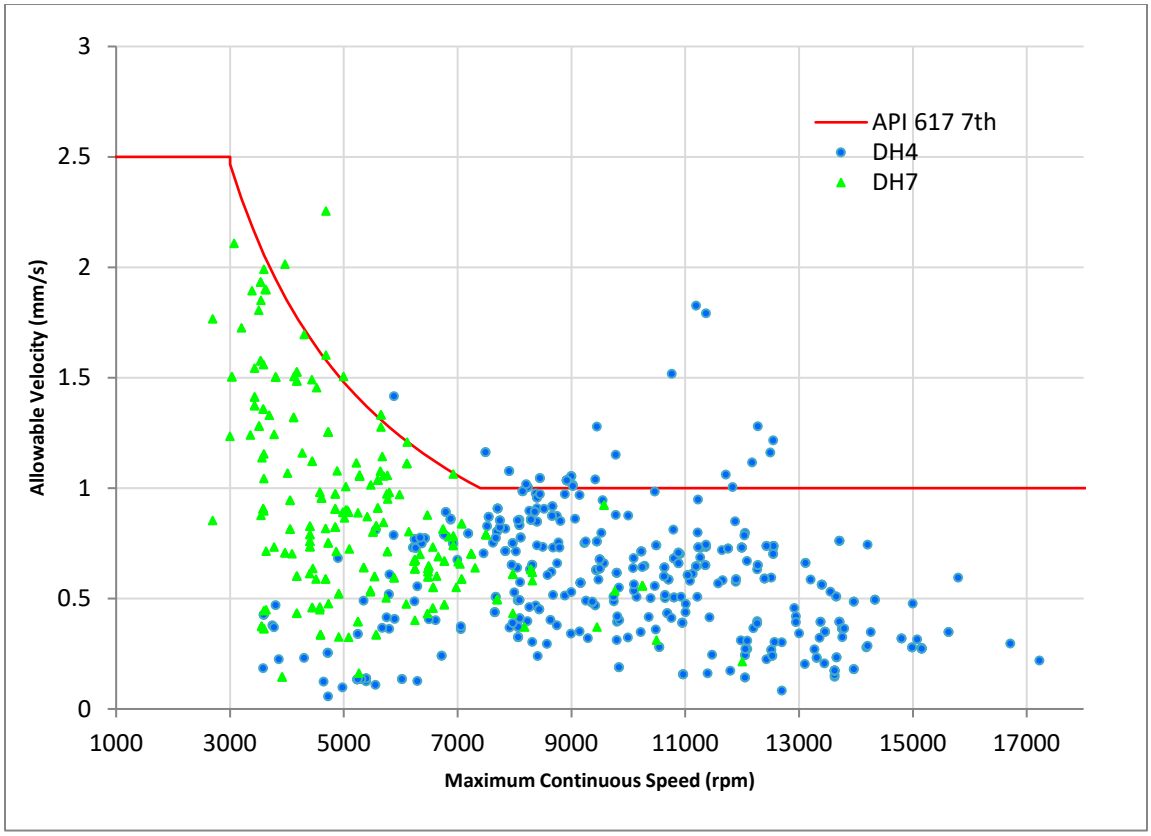

Figure 3: MCS vs. Allowable Velocity with shop order data

For some of the V1 criteria, such API 687, 1st Edition, velocity "measured on the bearing cap" is also specified. This might be difficult to comply with because the velocimeters are often located (built-in) below the bearing housing in the pedestals.

D1, the displacement criteria, is only used in API 612, 7th edition, and it is similar to the criteria used in shop tests (or test floor tests), only tighter. The commonly used shop tests acceptance criteria are in the following format (SI units):

$$A = 25.4\sqrt{\frac{12000}{N}} \qquad (3)$$

where

A is amplitude (μm)
N is the maximum continuous speed, in rpm

The vibration amplitude (unfiltered) measured by any probe (of the four) should not exceed A or 25.4 μm within the operating speed range.

Comparing to the shop test acceptance criteria, D1 is using the 1X filtered data, which are smaller than the unfiltered values, but the 25.4 μm limit at any response might be difficult to comply with at the first critical speed and trip speed. The 12.7 μm limit for the operating range is a reasonable target to try, but it might not be achievable in some instances. For example, the support stiffness might lower the second critical speed into the operating speed range.

Although both velocity and displacement measurements are available in balancing facilities, the velocity measurement is usually used for balancing and balancing criteria because of the relative stable situation: the velocimeters are built-in within the pedestals so the quality of measurement stays the same regardless the rotor being balanced. The eddy-current probes might be shifted depending on the rotor and bearing combination. Sometimes the probes might not even be at a burnished area.

If the probe location at the balancing facility is different from the actual machine location due to the bearing housing configuration, a multiplier can be used to adjust the acceptance criteria as suggested in ISO 11342, Section 8.2.5. The value of the multiplier can be derived by comparing the vibration amplitudes at the two locations by doing rotordynamic analysis (note that the value depends on the rotor modal characteristics and speed, so it needs to be established for each specific application). If the probes are not at the burnished area, the quality of the measurement could be too poor to be useful.

PEDESTAL DYNAMICS

Originally, an outside consulting firm (Consultant) was brought in to perform these modal tests to obtain improved pedestal transfer functions. However, after repeating the test with Elliott equipment, the pedestal responses did not agree within expectations. *Figure 4* and *Figure 5* show examples of the differences seen on the DH4 pedestals. Large differences in peak location and amplitude were also seen on the DH7 pedestals. It is important to note that Consultant was not asked to perform measurements at several pedestal locations along the rails, or to troubleshoot any pedestal setup, despite the knowledge that this could have an impact on measurement repeatability. The original report provided by Consultant included the pedestal locations for all measurements for this reason, as any troubleshooting of the bunker setup and repeatability was the responsibility of Elliott.

The labels for the FRF directions indicate the measurement direction and the direction of the hit, in that order. For example, the "XY" measurement indicates a response measured in the horizontal (X) direction due to an impact in the vertical (Y) direction.

Each pedestal has additional hydraulically actuated stiffening devices. These auxiliary supports are parallel to the main supports and provide additional stiffness when activated. This is referred to as the "stiffening on" setting, whereas the "stiffening off" setting refers to the base pedestal stiffness without auxiliary support.

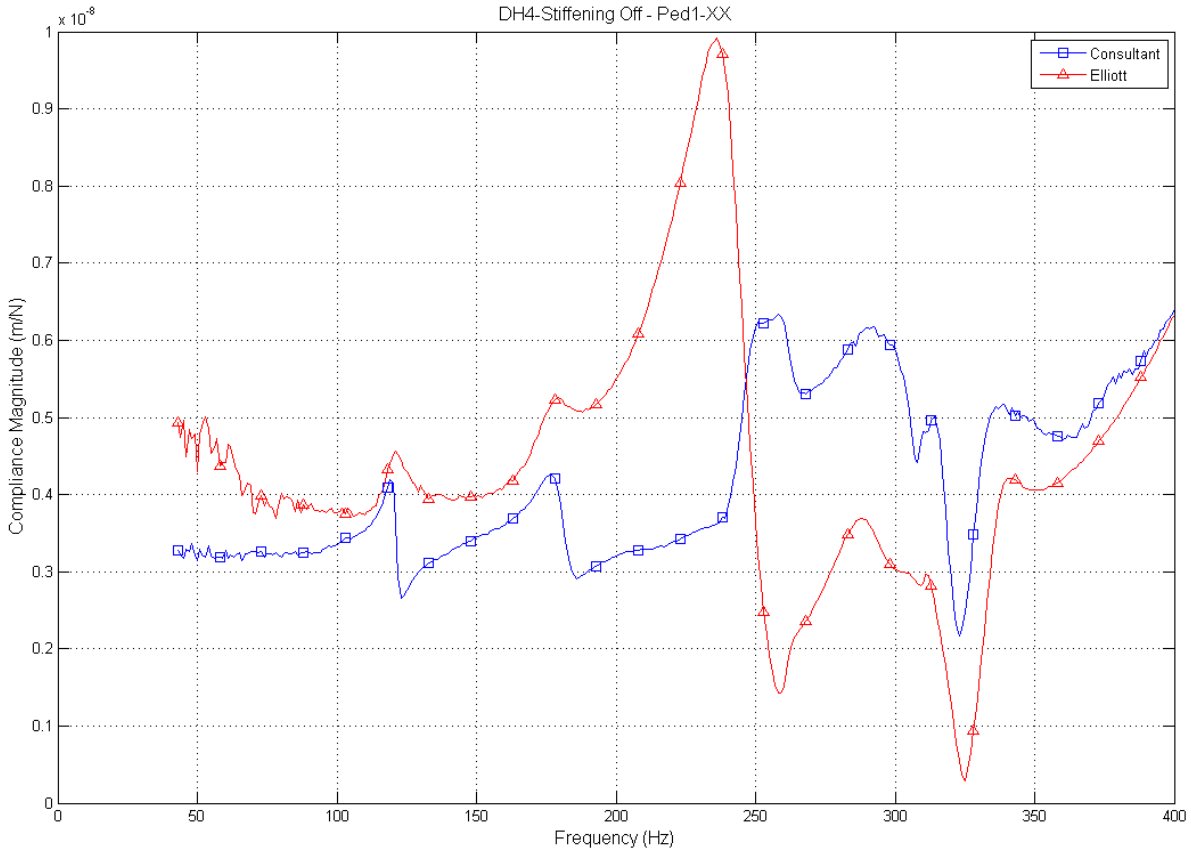

Figure 4: Consultant vs Internal Compliance Measurements on DH4 Pedestal 1 – Stiffening Off – XX

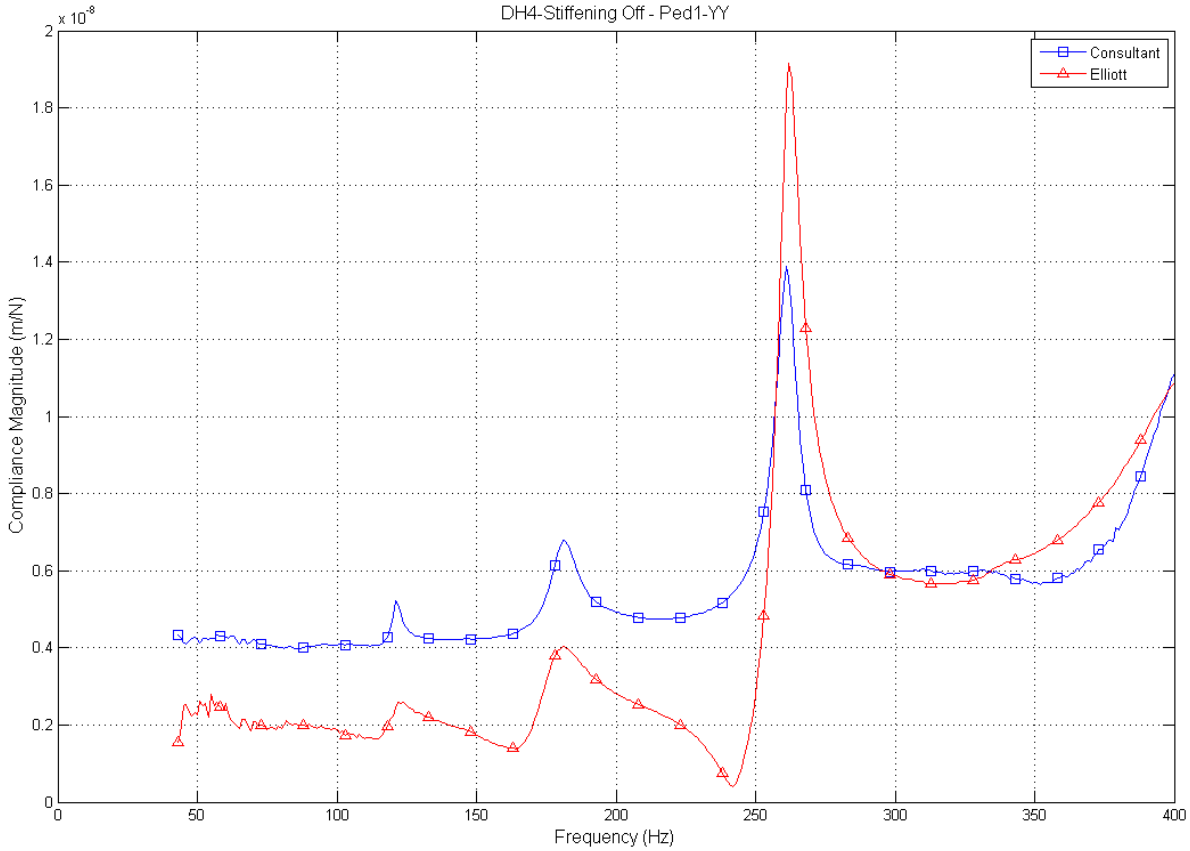

Figure 5: Consultant vs Internal Compliance Measurements on DH4 Pedestal 1 – Stiffening Off – YY

These disagreements forced an investigation into the root cause of the inconsistent pedestal measurements, as detailed next.

Investigation of Modal Testing Inconsistencies

A series of steps were performed to determine the root cause of the discrepancies. For convenience, all investigations were performed with the pedestal stiffening off:

1. All Elliott modal testing equipment was calibrated. The test reports provided by Consultant included up to date calibration sheets.
2. FRFs were collected after the pedestals were moved along the rails at various positions, to determine the effect of pedestal position.
3. A full modal test was performed on the rails to determine if the rail stiffness was influencing the pedestal dynamics.
4. FRFs were collected while the pedestals were lifted and dropped multiple times in the same location. This was to determine if the pedestal placement was inconsistent.
5. FRFs were collected with various torque levels used on the pedestal bedbolts to determine if the bedbolt torque changed the pedestal dynamics.
6. FRFs were collected with different torque levels used on the bearing cap bolts to determine if the bearing cap bolt torque changed the pedestal dynamics.

Figure 6 shows the effect of moving the pedestals along the rails and repeating the measurements, while using the same equipment and setup for each measurement. The results show the pedestal dynamics changed significantly as the pedestals were moved. The legend indicates the distance (cm) of each pedestal to the end of the rails on the drive-end. At the time, it was not clear whether the location of each pedestal would affect the results as cross-talk between the two pedestals, so the locations of both pedestals are recorded (P1 as pedestal 1, and P2 as pedestal 2).

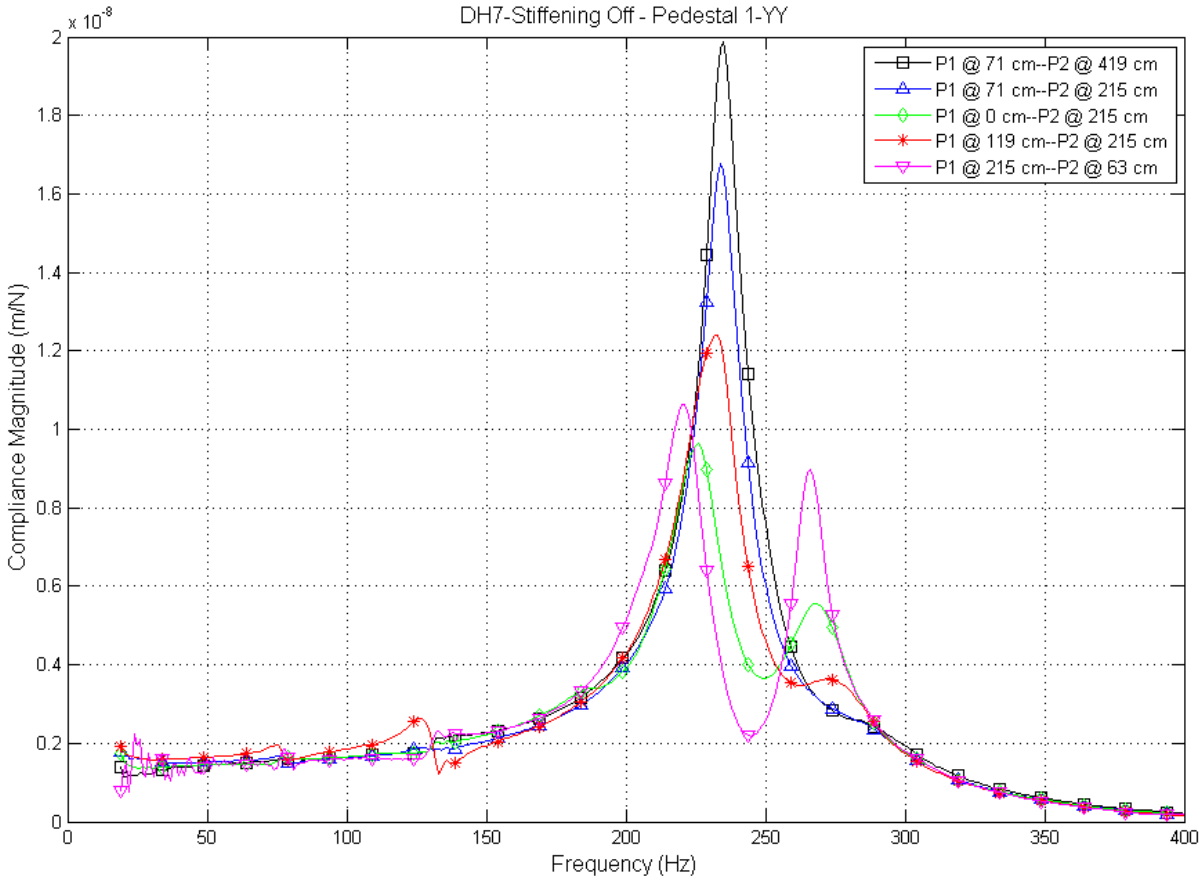

Figure 6: DH7 Pedestal Response at Various Rail Locations (YY)

To determine if the rails were interfering with the pedestal responses, a full modal test of the rails was performed. All pedestals were removed from the bunker during this test. No coherent response could be measured in the frequency range of interest using a 1 kg impact modal hammer, so it is believed that the rails were stiff enough and should not be interacting with the pedestal modes.

Figure 7 shows compliance measurements after lifting and repositioning the pedestal multiple times in the exact same location. This was to determine whether the act of lifting and placing the pedestal had any effect, which would indicate inconsistencies when securing the pedestals in place. Significant differences in pedestal response are apparent, particularly in the vertical direction, indicating that pedestal placement was inconsistent in some manner.

After acquiring all the confusing results, finally the torque on the bedbolts (the bolts that hold the pedestals to the rails) became the primary suspect. The bolts had been tightened “as tight as possible” by the operators, as no torque wrench was used in the past. A torque wrench was used for the following study, and the pedestal bedbolts were torqued to various levels. FRF measurements were taken at each torque level to document the different pedestal response to varying bolting torque. The pedestals were not moved throughout the entire test to rule out all other possibilities. An example of the results in *Figure 8* indicates that bolting torque has a significant impact on pedestal response.

It is interesting to note that using a torque wrench significantly reduced the amplitude of the second vertical mode at approximately 275 Hz, for all the torques used. It is possible that this mode is influenced by inconsistent bolting torque between each bolt, rather than an overall torque used for all bolts. When operators tighten bolts by hand, the bolting torque can vary significantly across all bedbolts, whereas a torque wrench provides much greater consistency for each bolt on the pedestal.

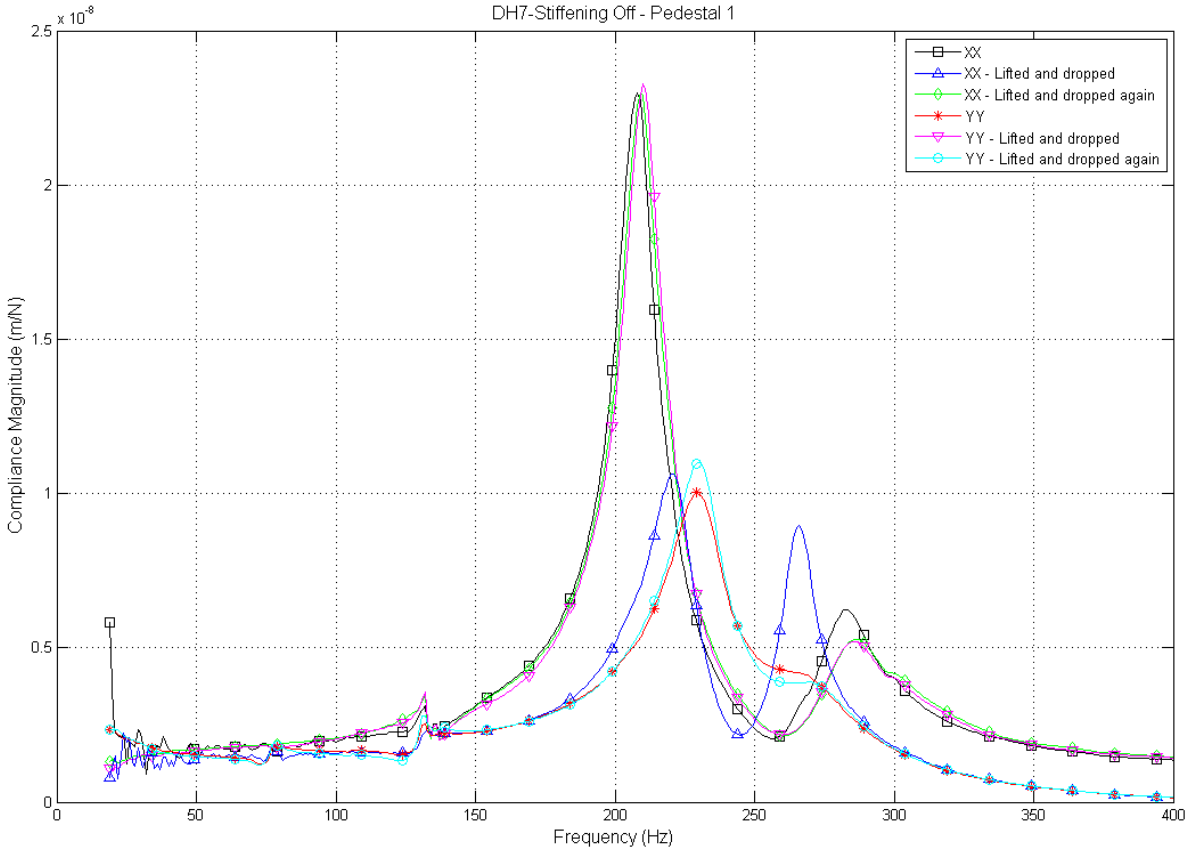

Figure 7: Effect of Pedestal Placement on FRF Measurements

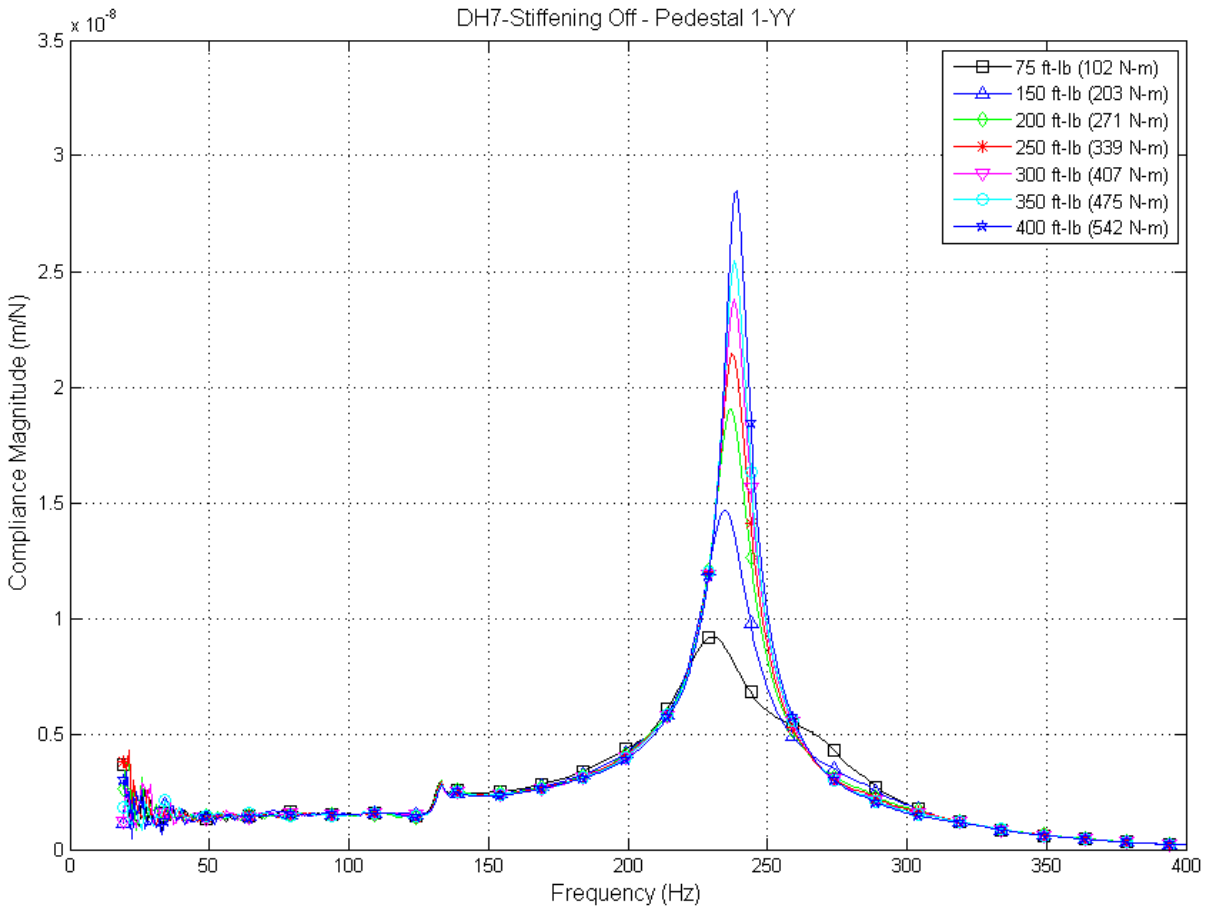

Figure 8: DH7 Pedestal Response to Varying Bedbolt Torque (YY)

As an additional check, the pedestals were moved to various locations while keeping the bolting torque consistent. A bolting torque of 250 ft-lb (339 N-m) was used for all pedestal locations. *Figure 9* confirms that a consistent bolting torque greatly improves repeatability of measured FRFs, regardless of pedestal location. As a comparison, a loosened case is also presented in the figure as the red-asterisked line.

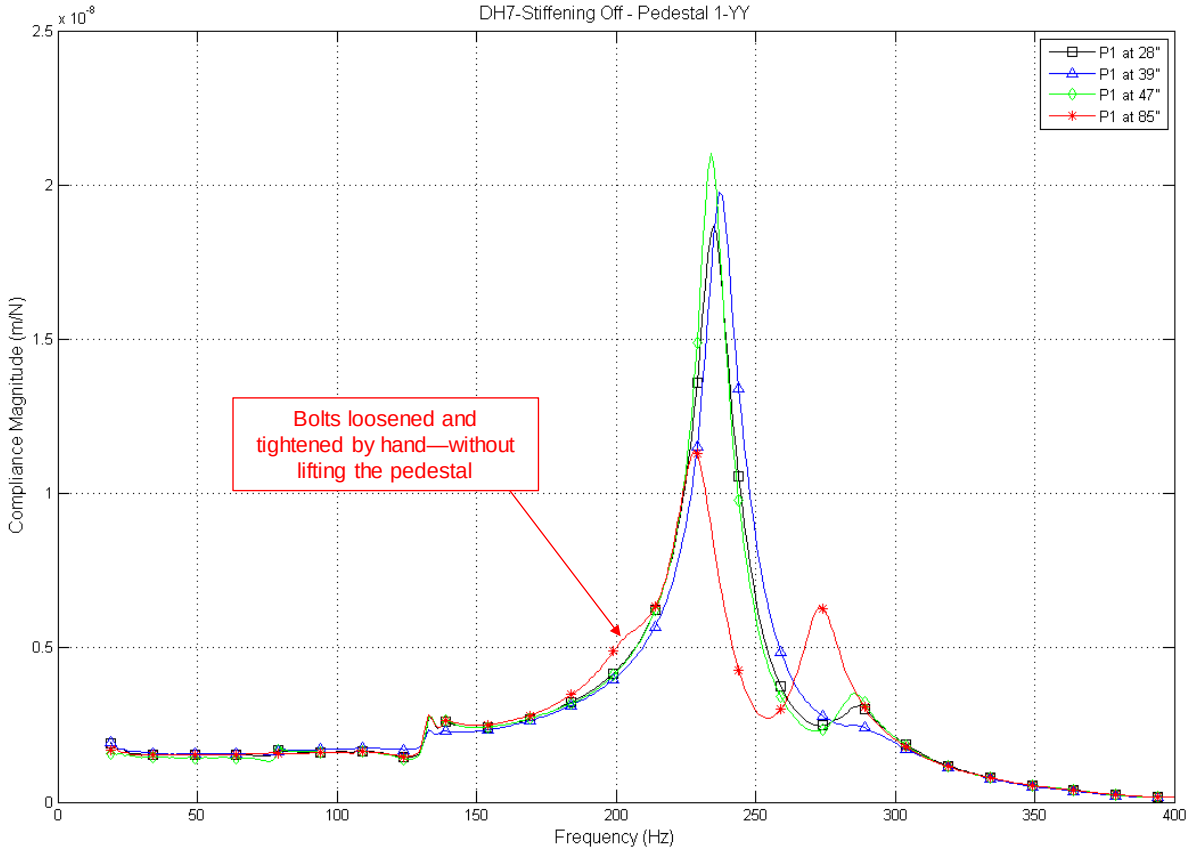

Figure 9: DH7 Pedestal Response at Various Rail Locations with Consistent Bedbolt Torque (YY)

Figure 10 shows a DH7 pedestal response with loosened and tightened bearing caps. At the time, a torque wrench for the bearing cap bolts was not available; therefore this was only a qualitative assessment. The results indicate that the bearing cap bolting torque presents a negligible impact on the pedestal response in the frequency range of interest. This test was repeated on the DH4 pedestals with similar results.

Although the bearing cap bolting torque does not appear to introduce any significant differences in compliance measurements under the test conditions, this was only a cursory assessment. The cap bolts may impact overall stiffness during operation and should always be tightened to the designed torque.

Alternate DH4 Impact Location

As an additional study into the effects of hammer impact location, FRFs were collected for the DH4 pedestals with an alternate horizontal impact location. The original impact location was directly next to the bearing location. The impact locations are shown in *Figure 11*. This alternate location was chosen because it should not introduce any axial / yaw excitation that can occur due to limited impact space near the bearing location.

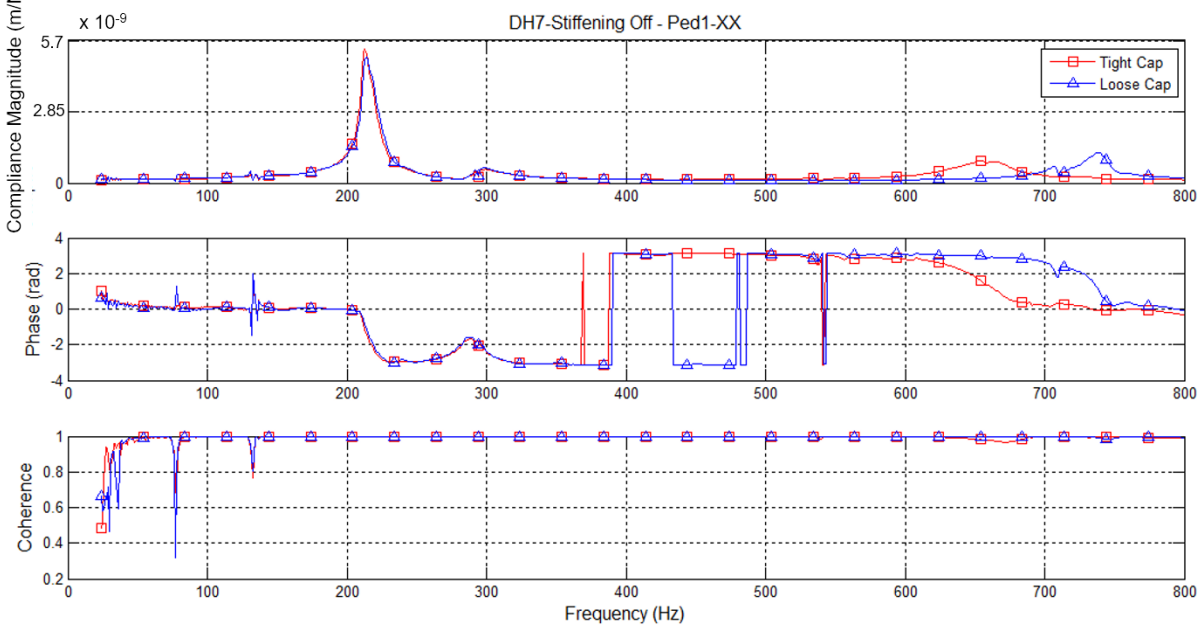

Figure 10: Effect of Loosened Bearing Cap Bolts on DH7 Pedestal 1 (XX)

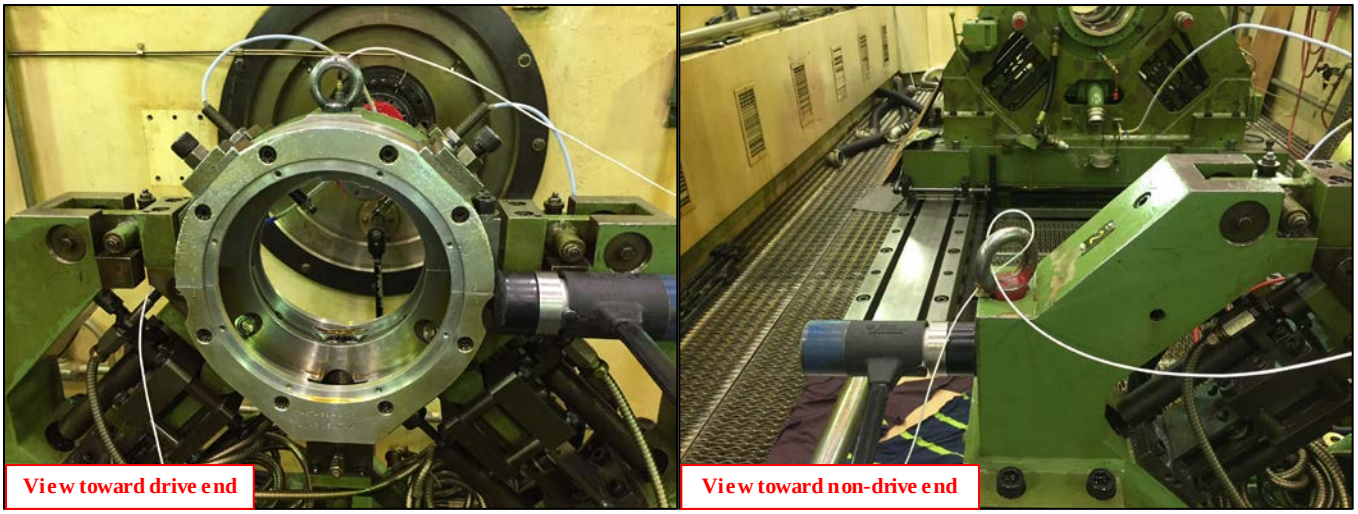

Figure 11: Original impact location (left) and alternate horizontal impact location (right) for DH4 pedestals

The horizontal responses measured from this alternate impact location for stiffening-off are provided in *Figure 12*. The vertical direction and stiffening-on cases show similar discrepancies: while this location successfully removes the low frequency axial mode excitations, the compliance magnitude is approximately an order of magnitude lower. Therefore, an impact excitation far away from the bearing location is not recommended for modal tests, as the pedestal stiffness could be greatly overestimated.

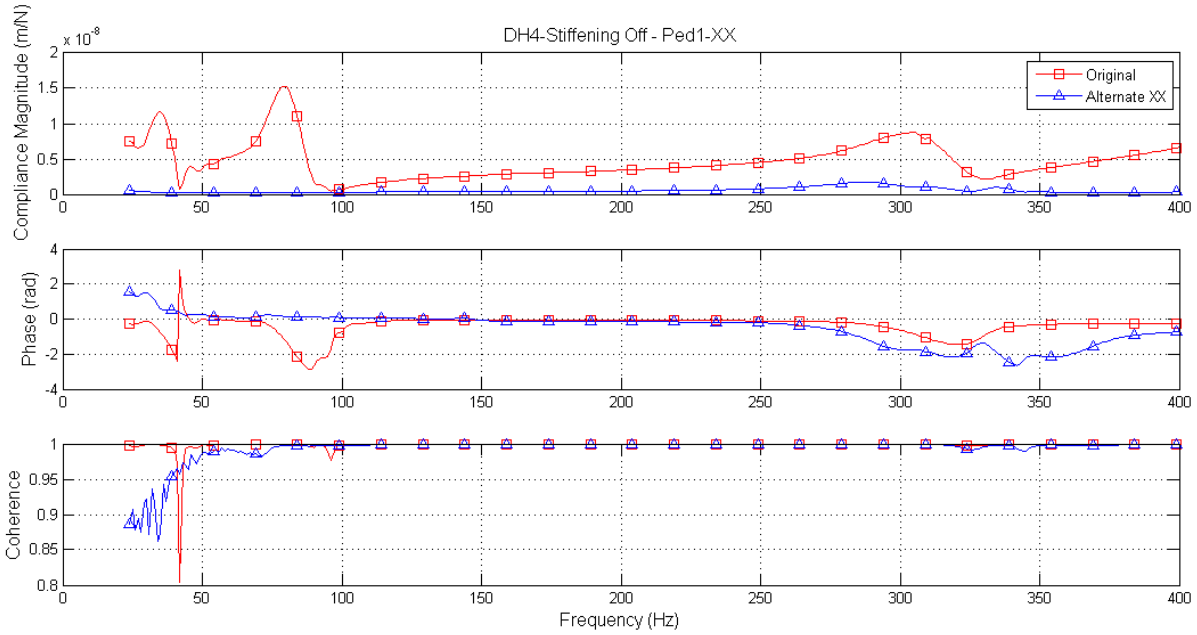

Figure 12: Response Comparison to Alternate Impact Location - DH4 - Stiffening Off - Pedestal 1 - XX

The investigations presented previously explore several possibilities to explain the measurement inconsistencies seen for the pedestals. The results indicate that the most important parameter to have a consistent result is the torque of the bedbolts, and the torque could be quite inconsistent even if the operators might feel otherwise. While there may be other contributing factors in inconsistent measurements (e.g. pedestal cross-talk), the inconsistent bedbolt torque has been demonstrated to be a major factor driving inconsistent modal test results. A pneumatic torque wrench was then obtained and used for further tests and balancing, and 600 ft-lb (813 N-m) bed bolt torque suggested by the Vendor for DH70 is used for all pedestals.

Pedestal Original Manufacture (Vendor) Tests

The Vendor has come to the Balancing Facility and performed both FRF measurement and shaker test. The shaker test (the shaker assembly is used in the pedestal bore) is to obtain low frequency stiffness, and the natural frequencies are measured with a supplemental impact hammer test.

Table 2: Single Mass Models Provided By Vendor

	Stiffening Off			Stiffening On		
	m	*c*	*k*	*m*	*c*	*k*
	kg	*N.s/μm*	*N/μm*	*kg*	*N.s/μm*	*N/μm*
DH4 PED1 - XX	20	1.8E-03	250	20	1.8E-03	560
DH4 PED1 - YY	20	1.8E-03	250	20	1.8E-03	560
DH4 PED2 - XX	20	1.8E-03	250	20	1.8E-03	560
DH4 PED2 - YY	20	1.8E-03	250	20	1.8E-03	560
DH7 PED1 - XX	349	1.8E-03	890	349	1.8E-03	1334
DH7 PED1 - YY	349	1.8E-03	890	349	1.8E-03	1334
DH7 PED2 - XX	349	1.8E-03	890	349	1.8E-03	1334
DH7 PED2 - YY	349	1.8E-03	890	349	1.8E-03	1334
DH70 PED1 - XX	810	1.8E-03	1168	810	1.8E-03	2268
DH70 PED1 - YY	810	1.8E-03	1168	810	1.8E-03	2268
DH70 PED2 - XX	805	1.8E-03	1168	805	1.8E-03	2364
DH70 PED2 - YY	805	1.8E-03	1168	805	1.8E-03	2364

The modal mass is calculated using the low frequency stiffness and location of the peak from the FRFs. The provided modal mass (*m*), damping (*c*), and stiffness (*k*) are list in *Table 2* for all pedestals. Note that horizontal and vertical are considered the same, and no cross-coupling stiffness or damping is considered. A minimal value has traditionally been assumed for damping since the raw FRF data is not provided by the Vendor.

An example of the shaker test result from the Vendor report is shown in *Figure 13*. The authors were not successful in acquiring the raw FRFs from the Vendor.

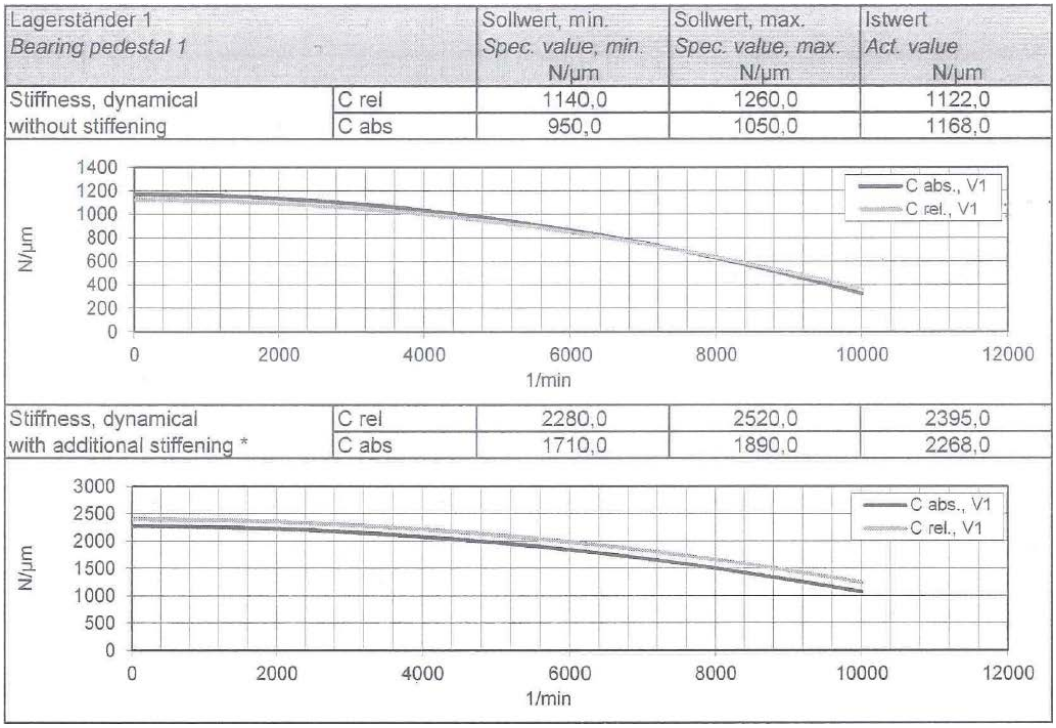

Figure 13: DH70 Shaker Test

DH7 Added-mass Test

The added-mass method (see Appendix A for details) can be used in the field or the test floor to check the pedestal stiffness, where the bearing cap often serves as the additional mass. For this study, a plug weighing 100 kg as shown in *Figure 14* was machined for the DH7 pedestal to create enough shift of the first critical speed / natural frequency.

As an example of the test results, the horizontal direction of stiffening-off case is shown in *Figure 15*. The calculation results are summarized in *Table 3*. The comparison will be carried out later together with other test results.

Table 3: Plug Test Results for DH7 Pedestals

	Stiffening Off			Stiffening On		
	m	*c*	*k*	*m*	*c*	*k*
	kg	*N.s/µm*	*N/µm*	*kg*	*N.s/µm*	*N/µm*
PED1 - XX	414	3.3E-02	755	560	5.8E-02	1159
PED1 - YY	311	1.7E-02	702	457	4.6E-02	1275
PED2 - XX	470	3.6E-02	881	823	8.5E-02	1786
PED2 - YY	322	1.4E-02	720	391	3.1E-02	1124

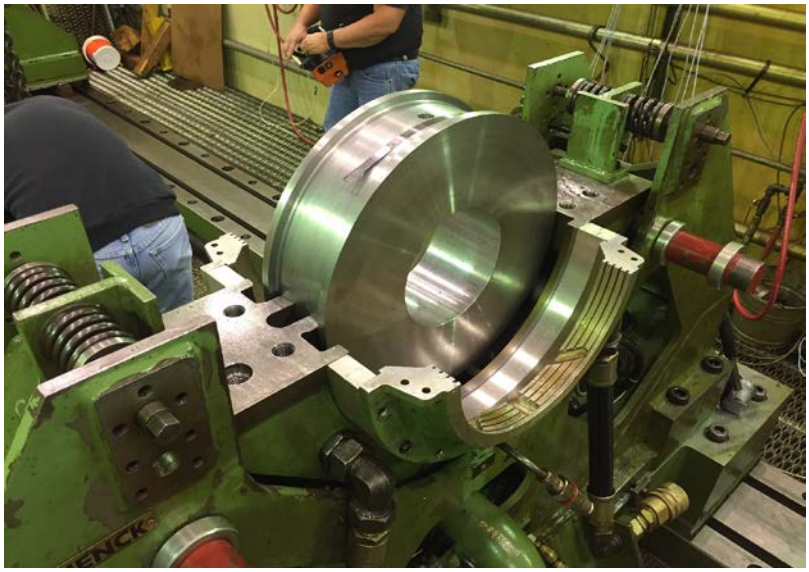

Figure 14: DH7 Pedestal Plug

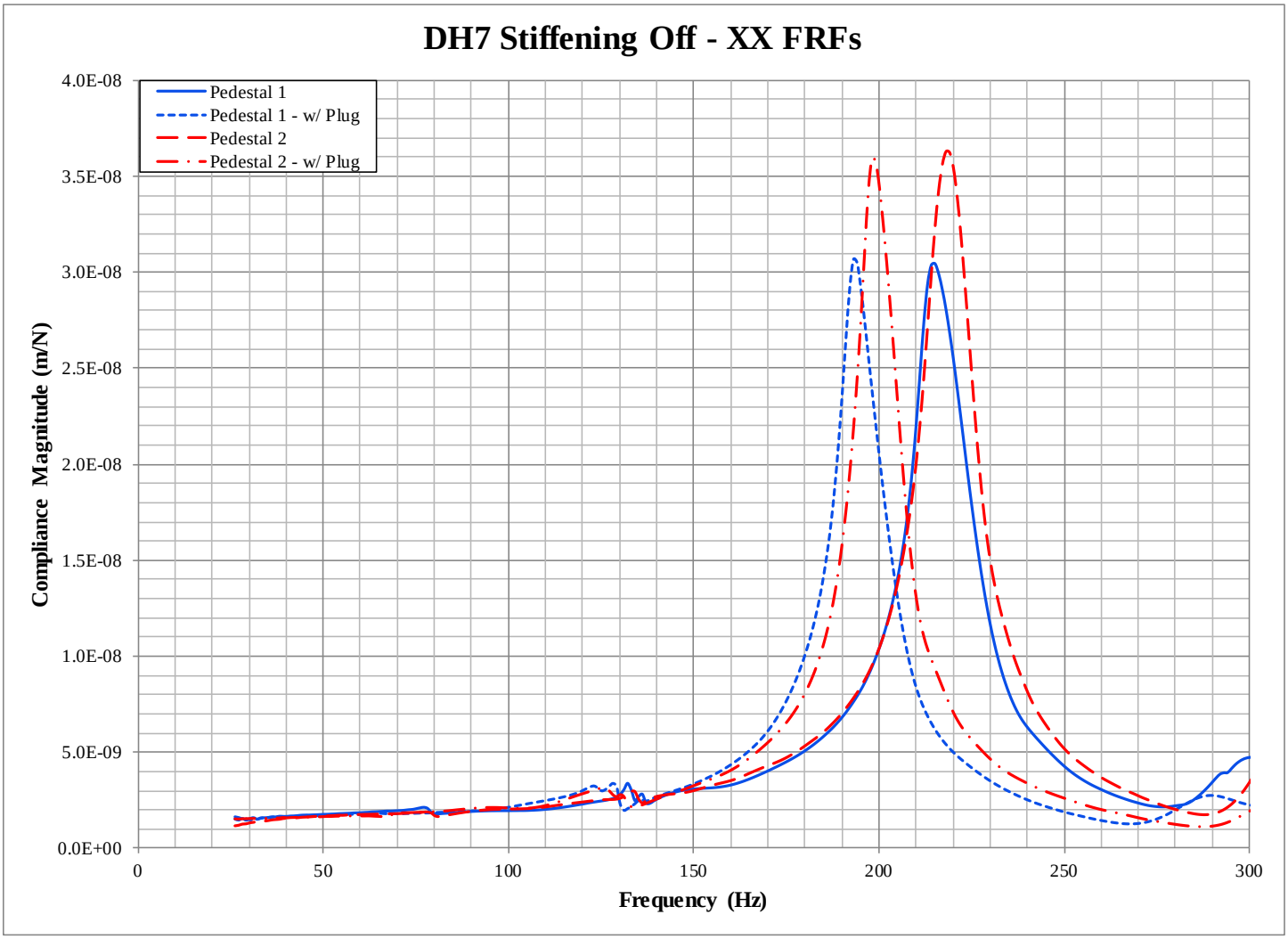

Figure 15: DH7 Pedestal Response with and without Plug (XX, Stiffening Off)

Modal Test Results

After all bolts were tightened to the specified values, modal measurements were performed for all pedestals with both stiffening on and

off.

The modal test setup is similar for all pedestals, as shown in *Figure 16* (accelerometer locations) and *Figure 17* (hammer location). Inside of the bearing housing was also tried as the locations of the accelerometers and hammer, but no significant difference was found.

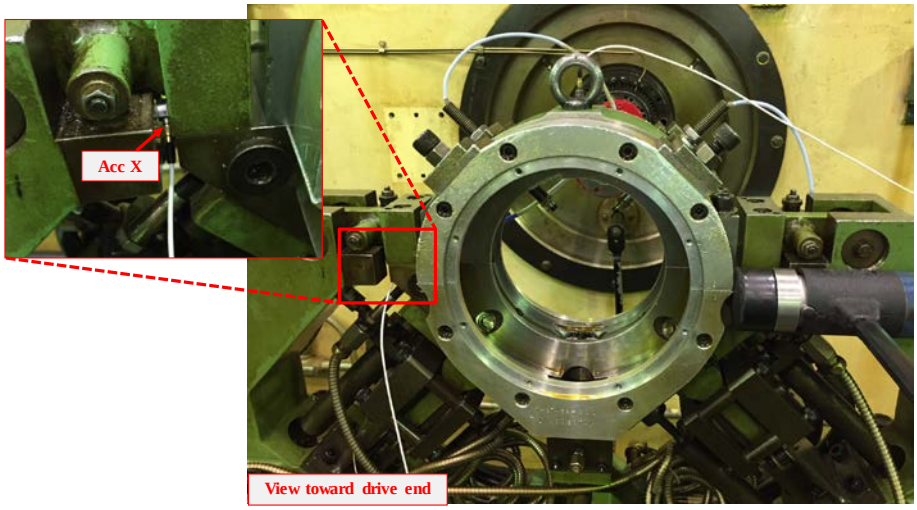

Figure 16: DH4 Horizontal Impact Location and Accelerometer Placement

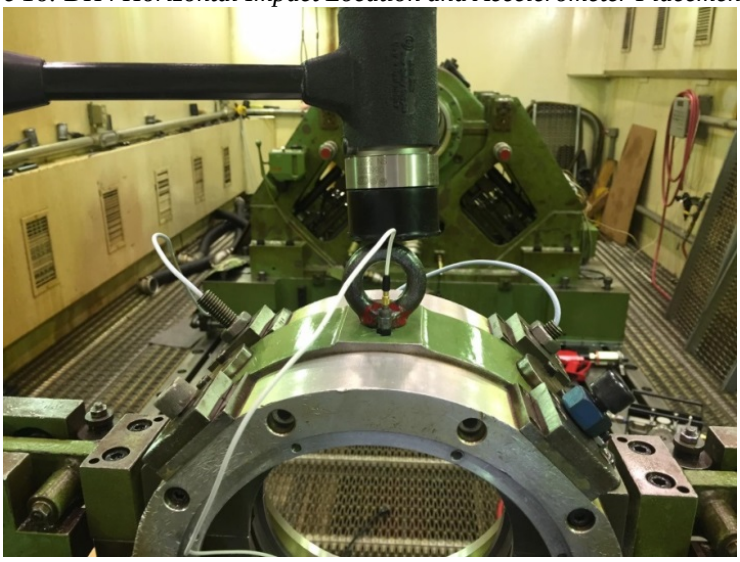

Figure 17: DH4 Vertical Impact Location and Accelerometer Placement

Mode shapes were also collected to help identifying the frequencies. A tri-axial accelerometer was placed at the top of the bearing cap, and a roving hammer technique was used. The frequencies of these modes were used in identifying the peak of interest when creating SDOF models from the FRFs. Note that the frequency may shift slightly when stiffening is used.

The measurements were then parameterized (curve-fitted) as either a single degree of freedom (SDOF) system or a multiple degree of freedom (MDOF) system. The SDOF is ideal because it can be used to compare the mass, damping and stiffness provided by the Vendor or measured with the added-mass method, but it may not be appropriate when multiple peaks exist in an FRF. Appendix B details the methods of the curve-fitting of the FRFs.

DH4 Pedestals

The modal parameters obtained for each direction are provided in *Table 4*, where the stiffness of the Vendor provided data are also presented as comparison. Note that because the peak for the YY direction is out of range of the measurement, the modal parameters (especially damping) cannot be identified accurately. Because the peak is out of range, the curve fitting will identify m, c, and k values that adequately model below the peak, but may not represent the actual peak.

Table 4: SDOF Model of DH4 Pedestals (Curve-Fit)

	Stiffening Off				Stiffening On			
	m	*c*	*k*	*k (Vendor)*	*m*	*c*	*k*	*k (Vendor)*
	kg	*N.s/µm*	*N/µm*		*kg*	*N.s/µm*	*N/µm*	
PED1 - XX	129	8.0E-02	471	250	257	2.4E-01	818	560
PED1 - YY	30	3.5E-05	296	250	47	1.1E-01	557	560
PED2 - XX	115	6.9E-02	413	250	167	1.8E-01	669	560
PED2 - YY	26	3.5E-05	256	250	99	1.7E-01	552	560

An example plot showing the amplitude of the measured FRFs is provided in *Figure 18*, where the frequency starts at 50 Hz because of the poor coherence below 50 Hz and also because the low frequency range is not a concern in general. There are two major peaks for the XX (horizontal) direction. The first peak (around 75 Hz) is demonstrated to be an axial mode by analyzing the mode shapes. Due to the imperfect hammer impact, the axial mode can be excited and reflected in the plot. This was verified by hitting different locations, and by reviewing the mode shapes of the corresponding frequencies.

The cross-coupling values are at least a magnitude smaller than the principal values for all pedestals, and therefore their contribution is not included in the tables. However, the cross-coupling was included in all identified models during analysis.

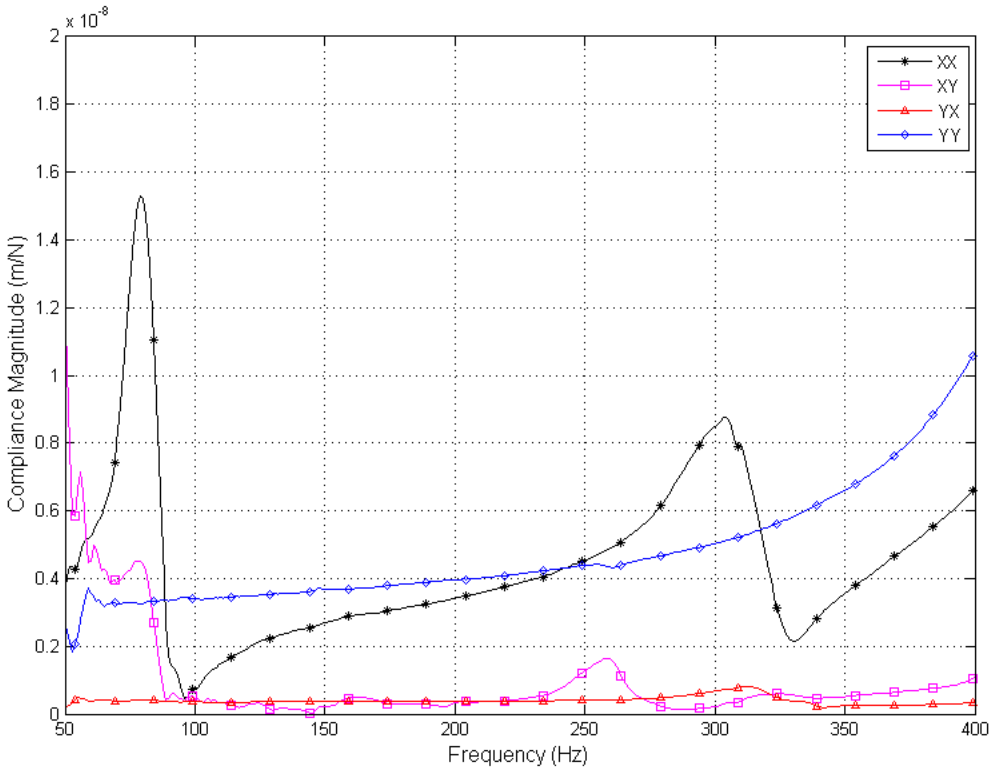

Figure 18: Measured FRFs for Pedestal 1 – Stiffening Off

An example plot showing the measured FRF and the model or curve-fitted data is provided in *Figure 19*, where the first two peaks were considered axial modes and then ignored in the curve-fitting. Note that for the Vendor provided data, the first peak is out of range of the display. Different models will be compared later on.

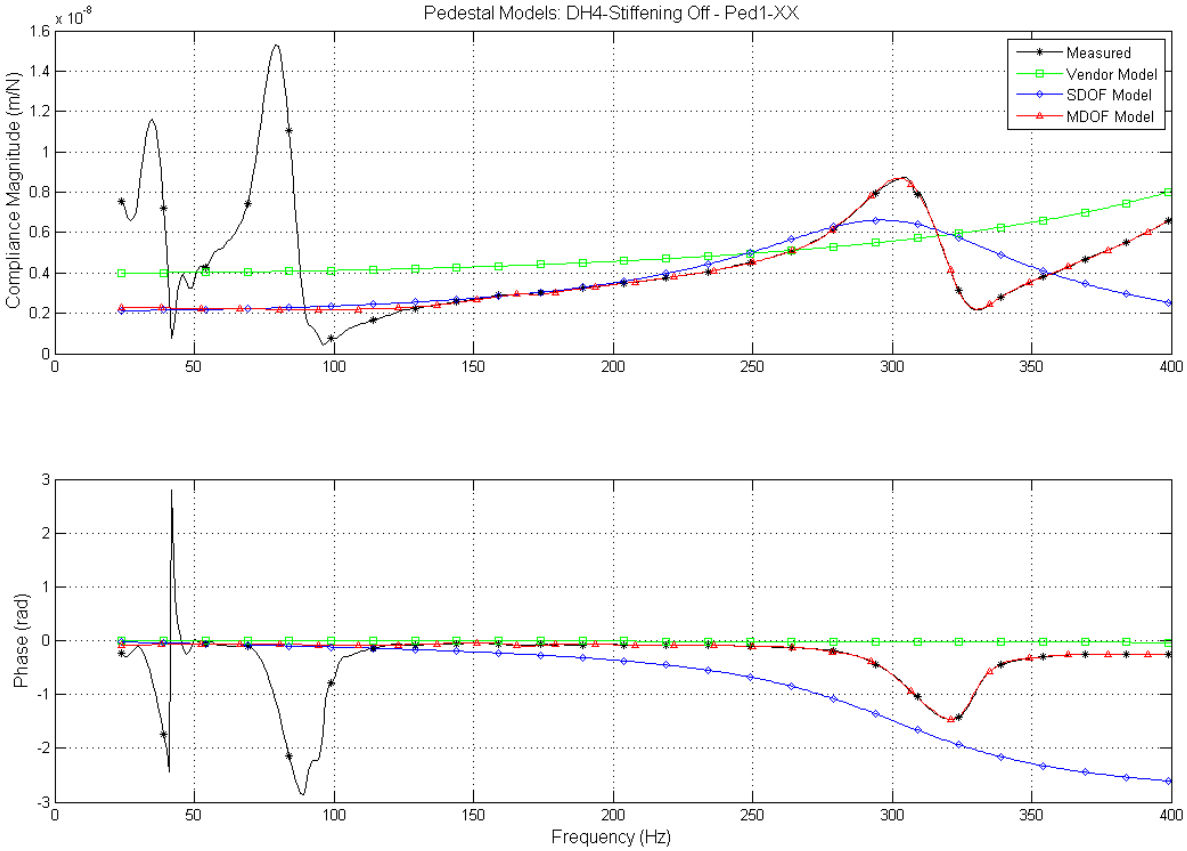

Figure 19: Measured vs Identified Models for DH4 - Pedestal 1 – Stiffening Off – XX

An example mode shape is provided in *Figure 20*.

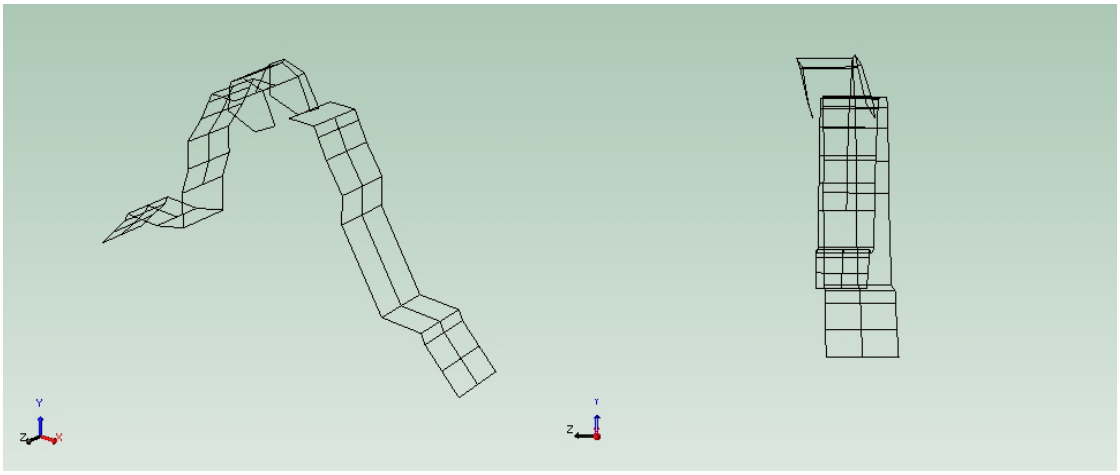

Figure 20: DH4 1st Axial Mode Shape - 38 Hz

DH7 Pedestals

The modal parameters identified for each direction are provided in *Table 5*, where the stiffness provided by the Vendor and the stiffness from the added-mass (Plug) test are also listed.

Table 5: SDOF Model of DH7 Pedestals (Curve-Fit)

	Stiffening Off					Stiffening On				
	m	*c*	*k*	*k (Vendor)*	*k (Plug)*	*m*	*c*	*k*	*k (Vendor)*	*k (Plug)*
	kg	*N.s/µm*	*N/µm*			*kg*	*N.s/µm*	*N/µm*		
PED1 - XX	324	2.4E-02	599	890	755	383	4.5E-02	797	1334	1159
PED1 - YY	399	2.2E-02	898	890	702	496	5.8E-02	1380	1334	1275
PED2 - XX	294	1.9E-02	553	890	881	341	3.5E-02	737	1334	1786
PED2 - YY	402	1.9E-02	904	890	720	475	4.4E-02	1354	1334	1124

An example plot showing the amplitude of the measured FRFs is provided in *Figure 21*.

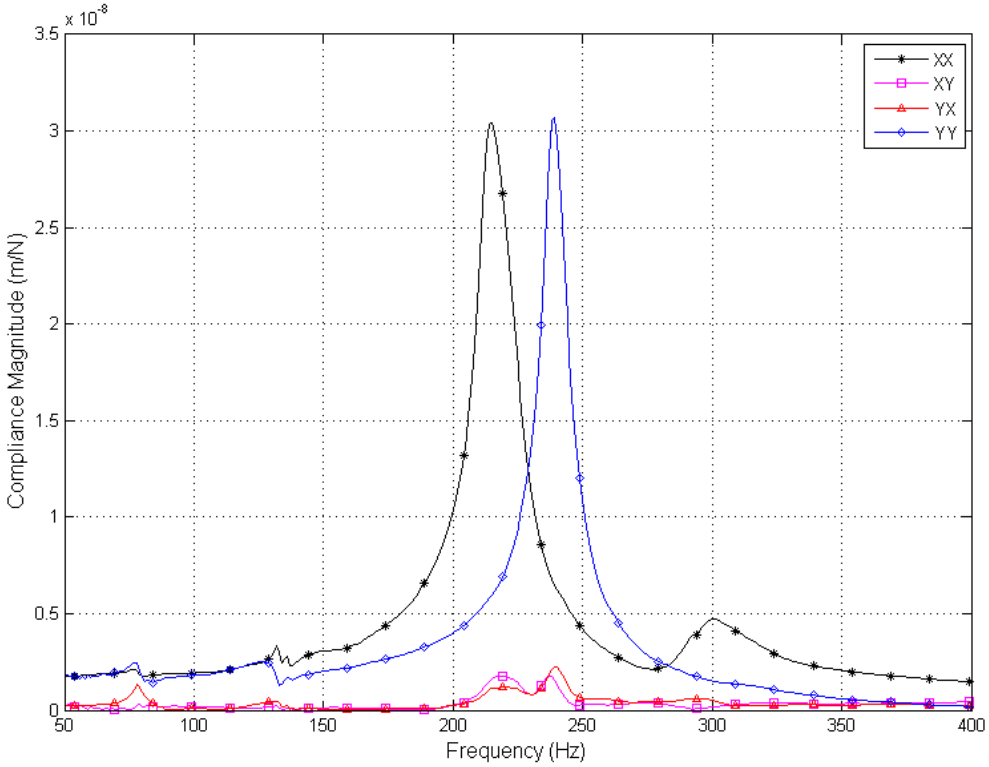

Figure 21: Measured FRFs for DH7 - Pedestal 1 – Stiffening Off

An example plot showing the measured FRF and the identified models is provided in *Figure 22*, where the model from the Vendor has a low damping value (1.8×10^{-3} N.s/µm), and therefore the peak is much higher and truncated.

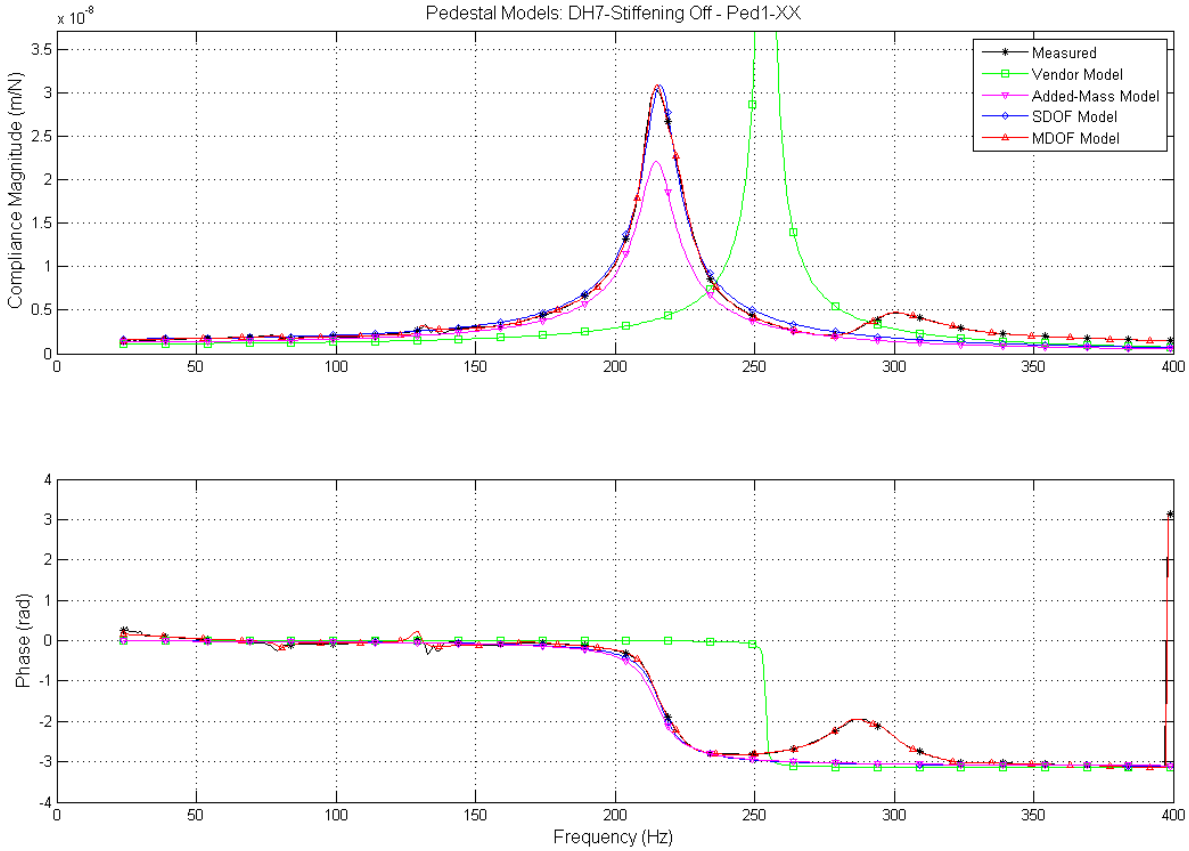

Figure 22: Measured vs Identified Models for DH7 - Pedestal 1 – Stiffening Off – XX

An example mode shape is shown in *Figure 23*.

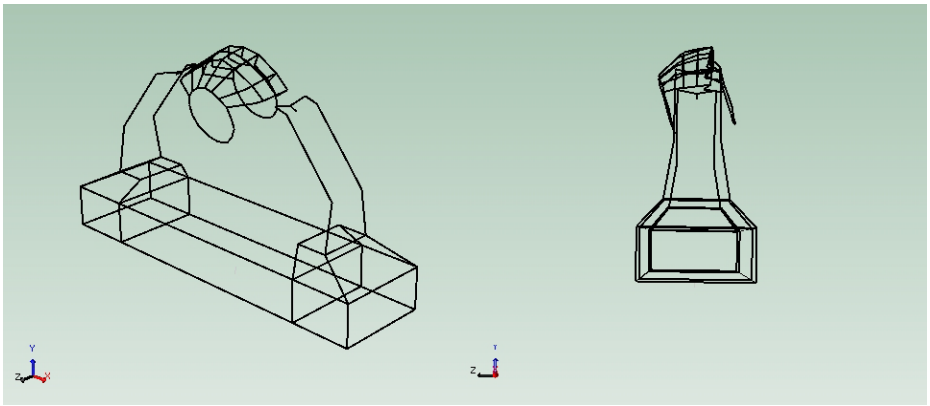

Figure 23: DH7 1st Axial Mode Shape - 129 Hz

The modal parameters obtained for each method are provided in *Table 6*, where the Vendor provided stiffness is also listed.

Table 6: SDOF Model of DH70 Pedestals (Curve-Fit)

	Stiffening off				Stiffening On			
	M	*c*	*k*	*k (Vendor)*	*m*	*c*	*k*	*k (Vendor)*
	kg	*N.s/µm*	*N/µm*		*kg*	*N.s/µm*	*N/µm*	
PED1 - XX	885	3.5E-02	963	1168	882	2.5E-02	1284	2268
PED1 - YY	805	3.1E-02	1322	1168	869	1.4E-01	1769	2268
PED2 - XX	792	3.6E-02	893	1168	953	3.9E-02	1401	2268
PED2 - YY	794	2.5E-02	1331	1168	848	2.1E-01	1665	2268

An example plot showing the compliance magnitude of the measured FRFs is provided in *Figure 24*. Note that there are three peaks in the XX direction, and multiple tests have been performed to confirm the measurement. The cause for multiple peaks in the XX direction is unknown. The authors were unsuccessful in acquiring further explanation or raw FRFs from the Vendor.

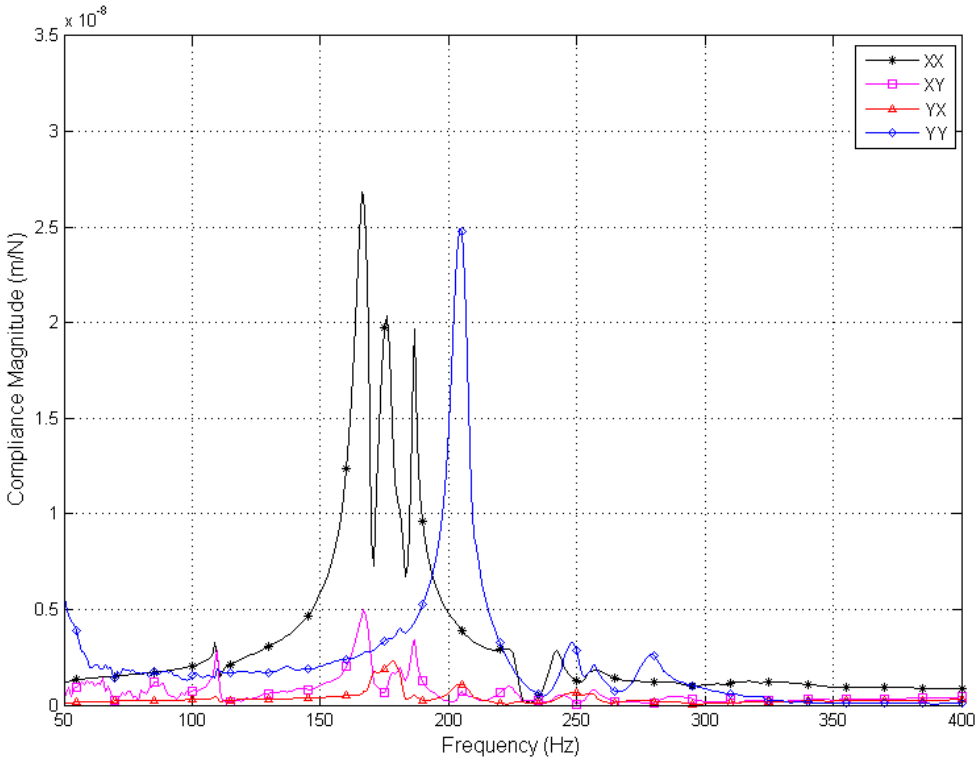

Figure 24: Measured FRFs for DH70 - Pedestal 1 – Stiffening Off

An example plot showing the measured FRF and the model or curve-fitted data is provided in *Figure 25*, where the FRF generated from the Vendor provided data has a low damping value (1.8×10^{-3} N.s/µm), and therefore the peak is much higher and truncated.

Due to time constraints of the Balancing Facility schedule, detailed mode shapes of the DH70 pedestals could not be collected. However, simplified mode shapes of a single row of points along the bearing cap were measured for a glimpse into the pedestal behavior, as shown in *Figure 26* for example, where arrows were used to help identifying the deformation directions within a single standing wave pattern.

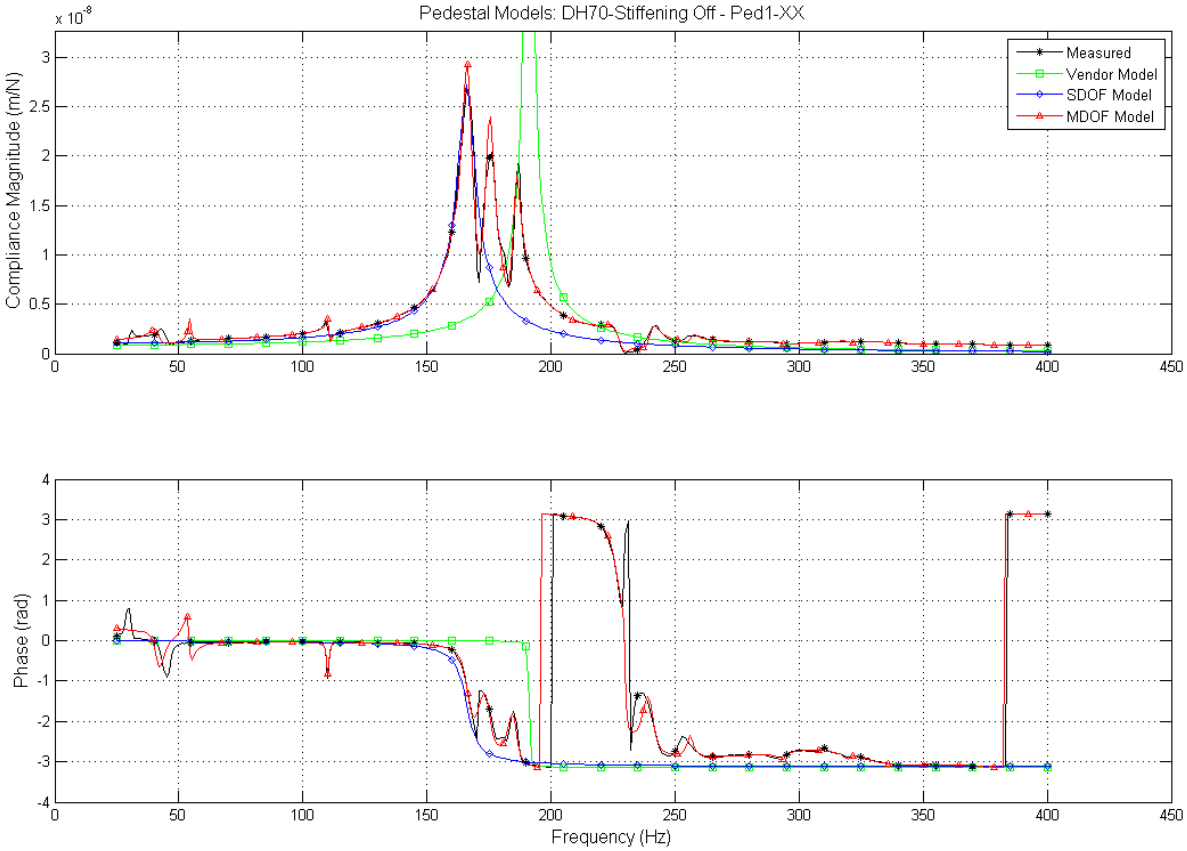

Figure 25: Measured vs Identified Models for DH70 - Pedestal 1 – Stiffening Off - XX

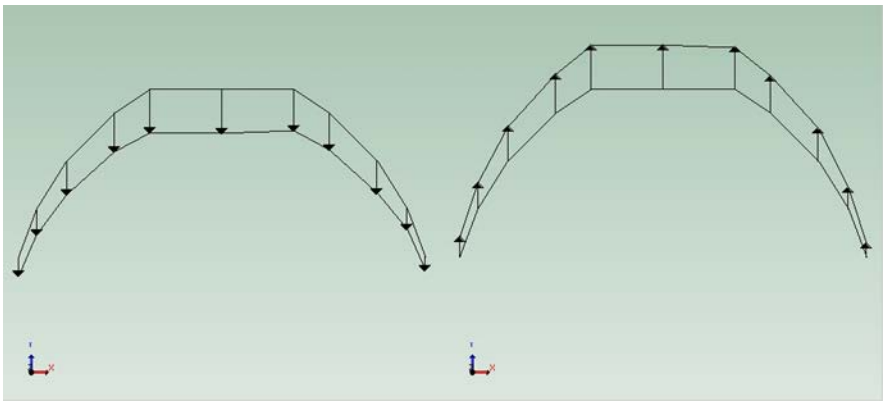

Figure 26: DH70 1st Vertical Mode Shape - 204 Hz

Discussion

From the measured FRFs, the following observations can be made:

1. The dynamics of different pedestals are largely different, e.g., DH7 has one clean peak within the concerned range while DH70 has multiple peaks.
2. The dynamics of the horizontal and vertical directions are different both in terms of peak locations and magnitude.
3. The cross-coupling dynamics is at least a magnitude smaller than the principal dynamics in this instance.

For the models, the following observations can be made:

1. The SDOF model, the Vendor model, and the Plug model are relatively close to each other.

2. Usually the Y (vertical) direction, different models have closer values (2-27% from the Vendor model stiffness). The discrepancies in the X (horizontal) direction are usually larger (14-88% from the Vendor model stiffness).

UNBALANCE VERIFICATION

With all the effort trying to obtain more accurate transfer functions as presented in the previous section, this section will show the results of implementing different types of pedestal models in the rotordynamics analyses of a shop order.

This shop order was balanced in the Balancing Facility and unbalance verification was performed with residual unbalance subtraction. For this method, one can see Nicholas (1997) for details. Later, the rotor was assembled into the compressor and passed the tests on the test floor. The unit was shipped to the field and successfully running.

The rotor, as shown in the figure below, is about 1650 kg with 6 x 3 inch bearings. In Balancing Facility, shop bearings were used with oil lift grooves at the two bottom pads. The unbalance verification tests were done with DH7 pedestals (stiffening on).

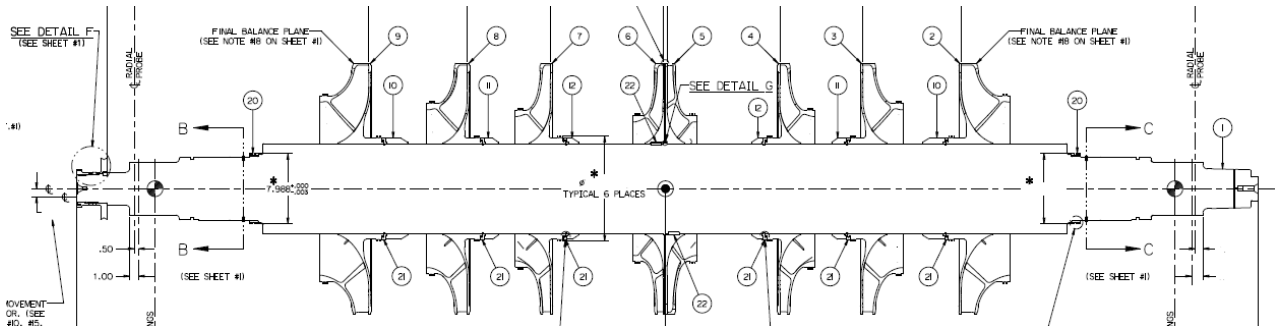

Figure 27: Rotor Cross-sectional Drawing

Standard bearing models were applied (measured bearing clearances and oil inlet temperature are used, but the oil lift grooves are not considered). The system was analyzed using different pedestal models. The mass of the bearing and bearing adapter is included in the analysis. The results are plotted in *Figure 28*, which shows:

1. There are no significant differences between different pedestal models.

2. All models predict higher first critical speed than the measured value (~200-300 rpm higher, 7-20% above the measured first critical speed), and lower than the rigid support (~100 rpm lower).

Although there is some improvement matching the measured response compared to the rigid support model, the improvement is not as much as expected. One of the first things needs to be checked is the rotor/bearing model, which was verified by the mechanical run data from the test floor. *Figure 29* shows the comparison between the prediction and the measurement from the test floor. Note that

1. The rotor is slightly different from the one used in the Balancing Facility, such as the dry gas seals and coupling.

2. The bearings are slightly different as well: the job bearings do not have the oil lift.

3. No support dynamics is used (infinite stiffness behind the bearings).

4. There is no unbalance verification done on the test floor, so the measured 1X uncompensated data shown in the figure is with the unknown residual unbalance. The same unbalance used in the analysis above is used for the test floor analysis.

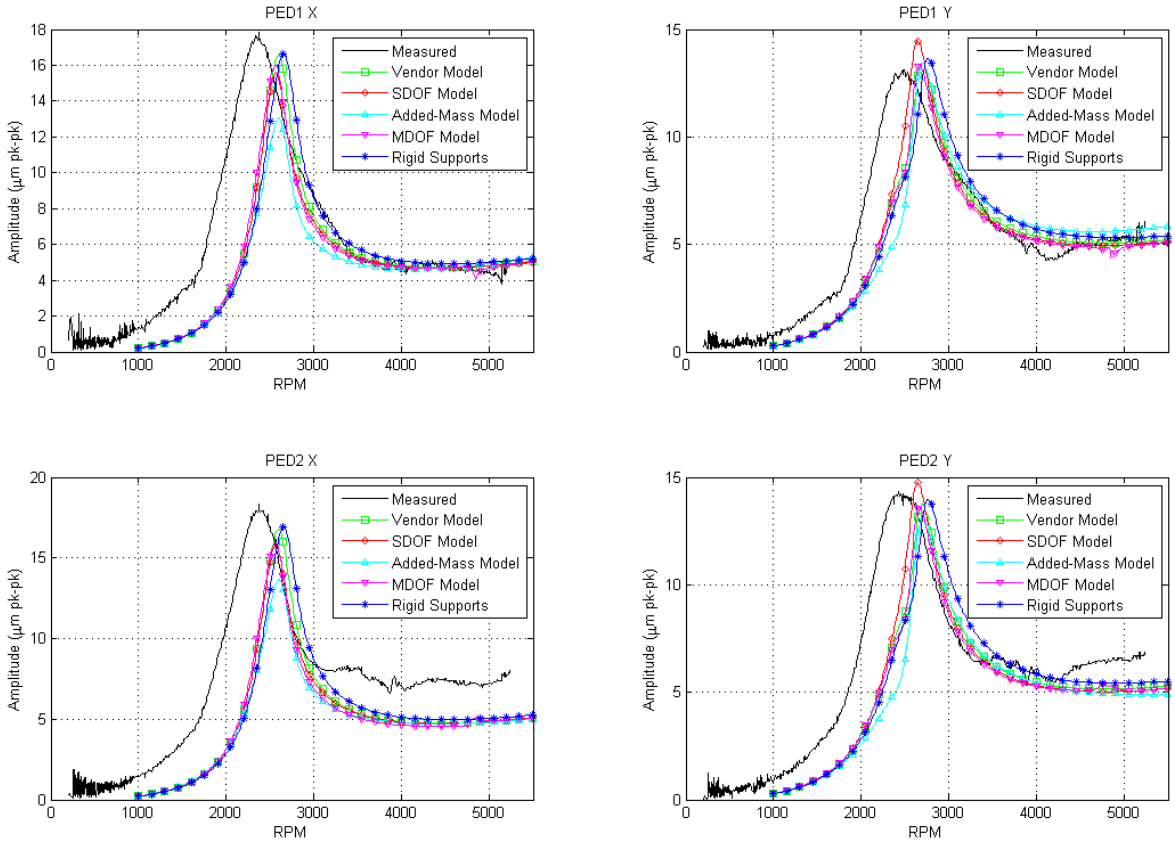

Figure 28: Unbalance Response Measurement vs. Prediction from Different Pedestal Models

The first peak location matches the measurement within 5% on the test floor.

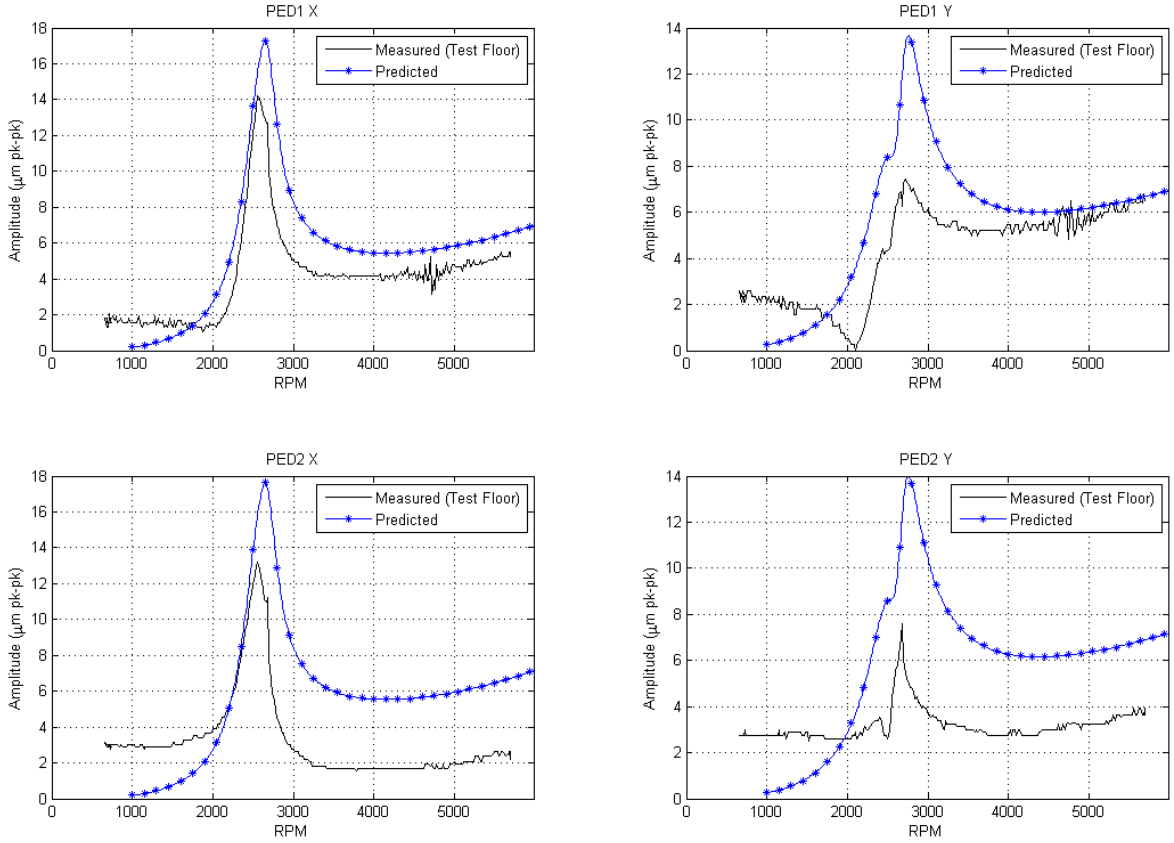

Figure 29: Test Floor Measurement vs. Prediction

Besides the pedestal dynamics, another factor, the oil lift, may have some unknown effects. For this particular study, the bearing dynamics (stiffness and damping) is adjusted to match the first peak (50% of the original values for all speeds is used for this particular case), and the result is shown in *Figure 30*, where the rigid support remains unchanged as a comparison. Note that even though the first peak matches better, the amplitude at higher speed deviates more. Therefore, the actual dynamics must be different in some manner.

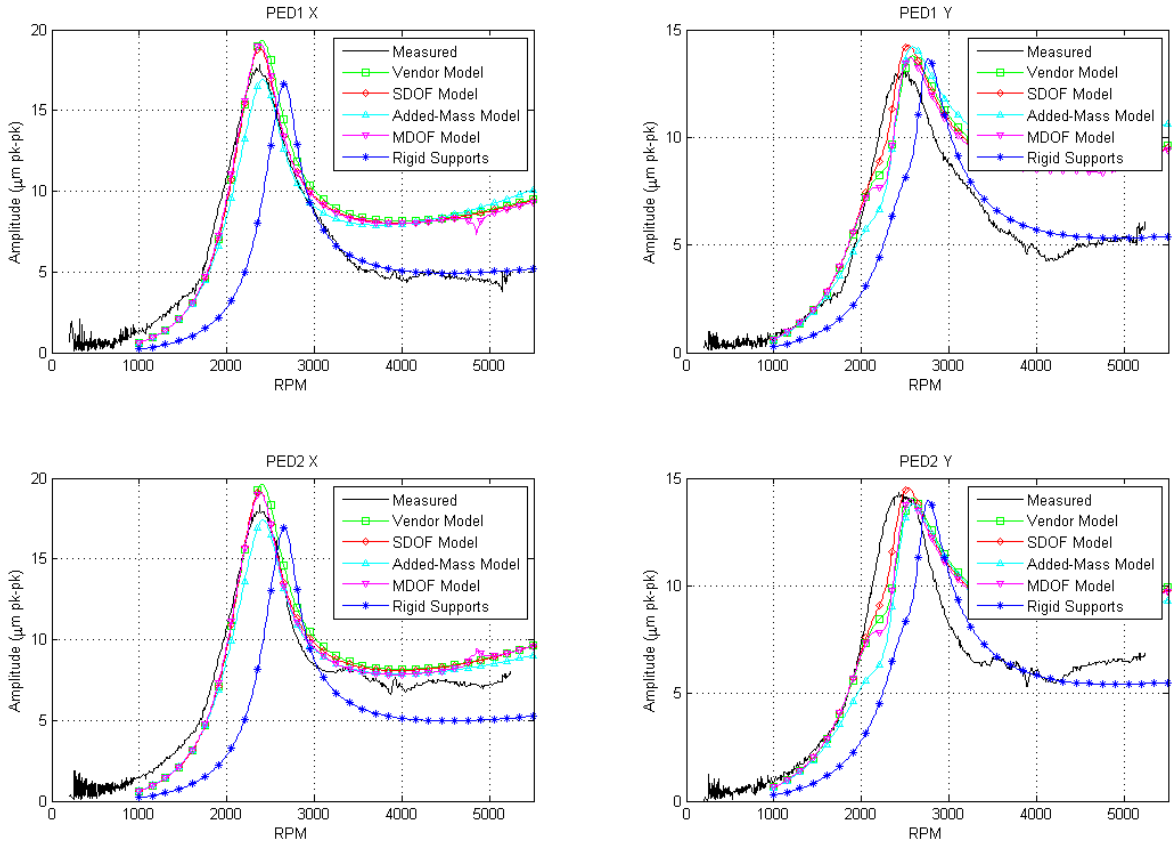

Figure 30: Measurement vs. Prediction with Bearing Adjustment

Table 7. Bearing Stiffness (Thrust End, Average Clearance)

Bearing Coefficients (N/µm)					
rpm	Kyy	Kxx	ωCyy	ωCxx	Somm.
1000	371.3	197.9	204.9	115.9	0.0067
2000	283.7	157.1	192.6	125.6	0.0741
3000	248.7	144.3	206.7	140.6	0.1415
3450	239.9	142.6	215.4	148.5	0.1752
4000	232.9	142.0	224.2	158.7	0.2157
5000	225.9	144.3	238.2	178.6	0.2763
5174	225.9	145.0	241.7	182.1	0.2898
6000	224.2	149.4	253.9	197.9	0.3487
7000	224.2	156.4	271.5	218.9	0.4111
8000	227.7	165.0	289.0	241.7	0.4785
9000	232.9	174.4	308.2	262.7	0.5459
10000	239.9	183.9	329.2	287.2	0.6133

Despite some rather large differences (e.g. mass and stiffness) between the pedestal models, all pedestal models yield quite similar rotordynamic results for this study in terms of both the critical speed and amplitude. The reason for this situation can be explained by the bearing coefficients shown in *Table 7*. The provided bearing coefficients are the nominal values before the adjustment.

In the concerned range, i.e. 2000-6000 rpm, the bearing stiffness is about 220 – 280 N/µm, while the stiffness of the pedestals from all

models are above 735 N/μm (near 3.5x the bearing stiffness specified by API 617) for DH7 stiff in both X and Y directions. Therefore the effect of the difference between models is not manifested in the particular case. For other cases where the bearing stiffness is higher relative to pedestal stiffness, large differences will show up.

Besides the shop order used above, the authors also compared the predictions of some other shop orders and almost all of them showed a higher predicted first critical speed, including the ones without oil lift grooves. It appears that the measured FRFs (or any method mentioned in this paper) are not matching the entire support dynamics (excluding bearings). An example for DH4 (no oil lift) is shown in *Figure 31* and *Figure 32*.

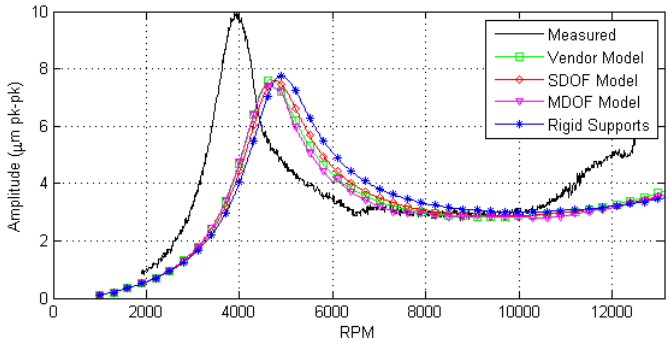

Figure 31: Measurement vs. Prediction forDH4

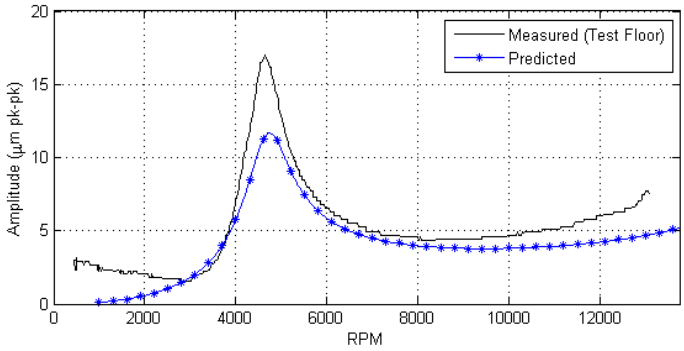

Figure 32: Test Floor Measurement vs. Prediction

Some possible reasons for the discrepancies between the models and support dynamics are listed below:

1. Non-linearity of the support, i.e., all measurements are obtained with rather small forces (~1-50 kgf), while the dynamics may change when shaking with a rotor (~500-5000 kg). The components that could have this non-linearity are:
    a. Bearing cap. This is unlike the reason once the bolts are properly tightened. The test floor data seem to indicate that bearing cap is not a problem.
    b. Pedestal. The 3 peaks in *Figure 24* indicate the complexity of the pedestal, so it is quite possible to have some non-linear dynamics.
    c. Foundation/rail. The difference between the foundation of the balancing facility and that of the test floor might not be significant in terms of e.g. stiffness, but since there is always a relatively large casing for the rotor on the test floor, the foundation influence might be less for the test floor than for the balancing facility.
    d. Varying bearing locations due to deviations in pedestal location during installing.
2. Incorrect bearing dynamics due to
    a. Hydrostatic lift grooves, when used, will alter the dynamic characteristics of the bearings. This may not have much effect, though, because for DH4 (no lift grooves) similar behavior is observed as shown in *Figure 31* and *Figure 32*.

VACUUM EFFECTS ON BEARING DYNAMICS AND FURTHER UNBALANCE VERIFICATION

The Balancing Facility usually runs rotors with vacuum to eliminate aerodynamic effects. Because the effect of this vacuum on the bearings and oil system was uncertain, a test rotor was spun with and without vacuum to measure the effects. This test is typically not possible due to the aerodynamic features of turbomachinery equipment, which adds significant thrust loading and heat if spun without vacuum.

For this test, a test rotor without blading was used. Three integral disks were machined in the center of the shaft. A diagram of the rotor is shown in *Figure 33*, and details of the rotor and test setup are listed in *Table 8*. Furthermore, an oil sample was taken from the Balancing Facility oil reservoir shortly after the tests. Third-party viscosity measurements were recorded for reference.

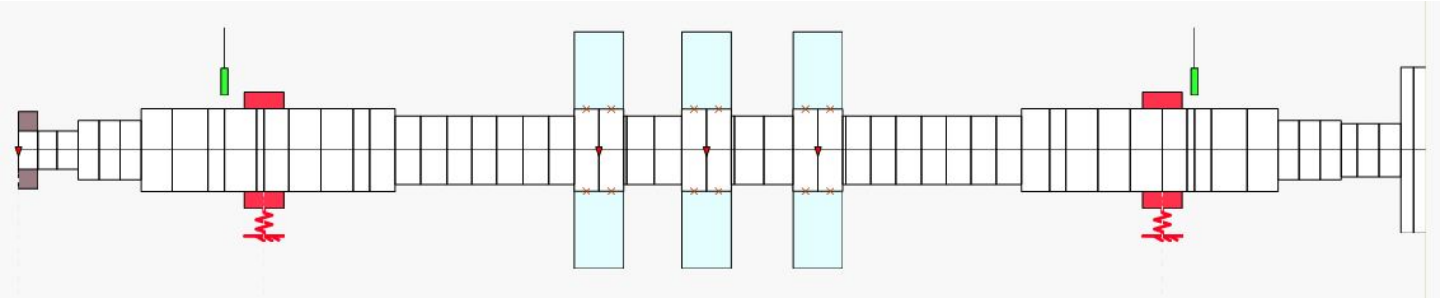

Figure 33: Test Rotor Used for Vacuum Tests

Table 8: Rotor and Test Parameters for Vacuum vs. Non-Vacuum Test

Rotor Weight, kgf.	108.8
Rotor Length, mm.	1445
Journal Diameter, mm.	89
Bearing Span, mm.	922
Bearing Diameter, mm.	89
Bearing Length, mm.	41
MCS, rpm	12,000
Drive Adapter Weight, kgf.	5.1
Lube Oil	ISO VG-32
Lube Oil Viscosity (cSt 40C)	36.0

Prior to spinning in the Balancing Facility, a modal test was performed on the rotor while suspended to verify the analytical model, as shown in *Figure 34*. A single-axis accelerometer was secured near the third disk, and a roving hammer technique was used to impact 16 points along the length of the rotor. The results of the modal test show agreement to the analytical model within 3% for the first two bending modes. The results are summarized in *Table 9*, and the predicted mode shapes are shown in *Figure 35*.

Figure 34: Suspended Test Rotor

Table 9: Modal Test Results of Test Rotor

Mode	Modal Test Frequency (Hz)	Calculated Frequency (Hz)	Difference (%)
1st Bending	132.9	129.4	-2.62
2nd Bending	368.6	367.7	-0.24

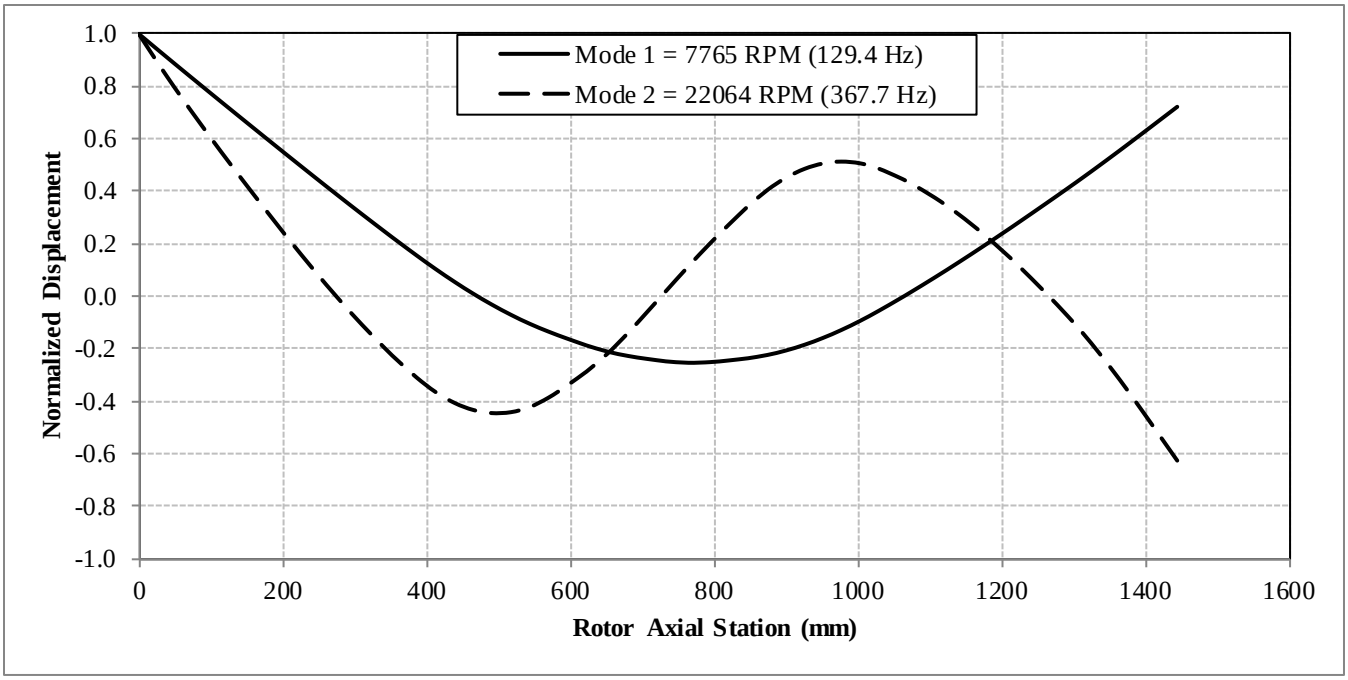

Figure 35: Predicted Mode Shapes of Test Rotor

Figure 36 shows the pedestal velocity measurements for both DH4 pedestals. Shaft displacement measurements are shown in *Figure 37*. As seen by the overlapping curves, it is clear that the vacuum had negligible effect on the system dynamics. Because the Balancing Facility oil system is flow-controlled, the only noticeable difference between the two runs was in the supply pressure required to maintain the same oil flow. The oil temperature rose slightly for the vacuum test, as this test was performed immediately after the non-vacuum test. The oil measurements for both tests are listed in *Table 10*.

Note that the rotor was only spun to 9,000 rpm instead of the designated MCS of 12,000 rpm out of caution. Despite not having aerodynamic blading, the disks had an abundance of balancing holes, which could have potentially generated significant heat at higher speeds. For this test, simply traversing the first critical speed was sufficient.

Table 10: Oil Measurements for Vacuum vs. Non-Vacuum Test

	Vacuum	No Vacuum
Oil Supply Temp, C	31	30
Oil Supply Pressure, Bar	2.90	3.65
Lube Oil Flow (Ped 1), L/min	13.6	13.6
Lube Oil Flow (Ped 2), L/min	13.6	13.6

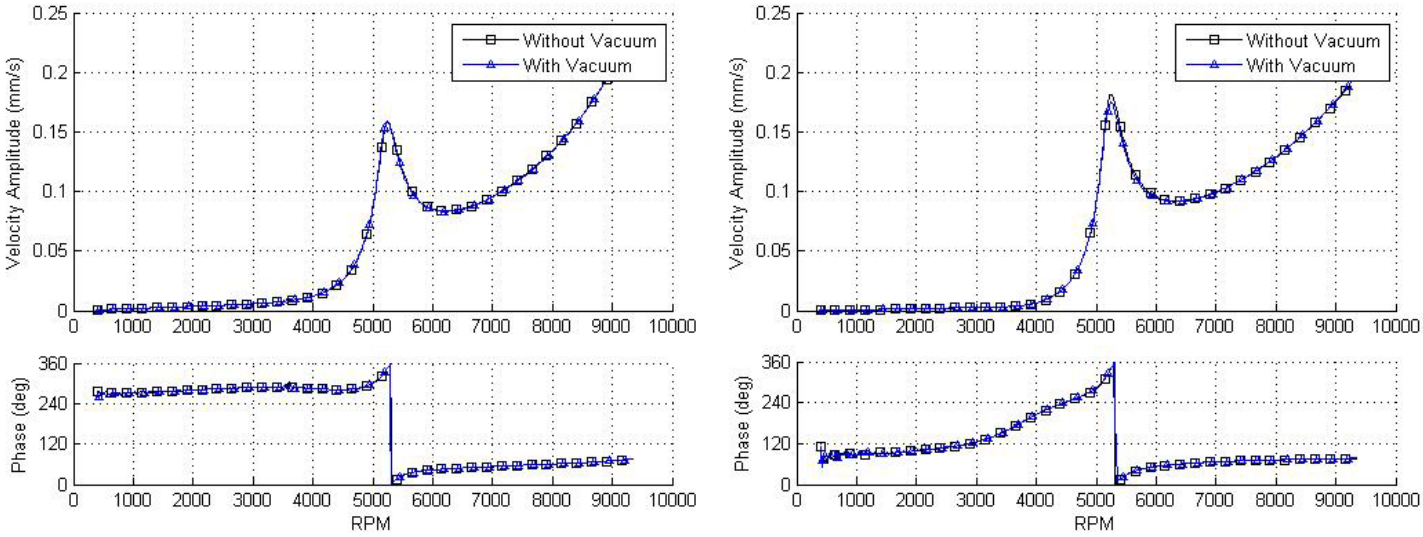

Figure 36: Pedestal Velocity Plots for Pedestal 1 (Left) and Pedestal 2 (Right) with and without Vacuum

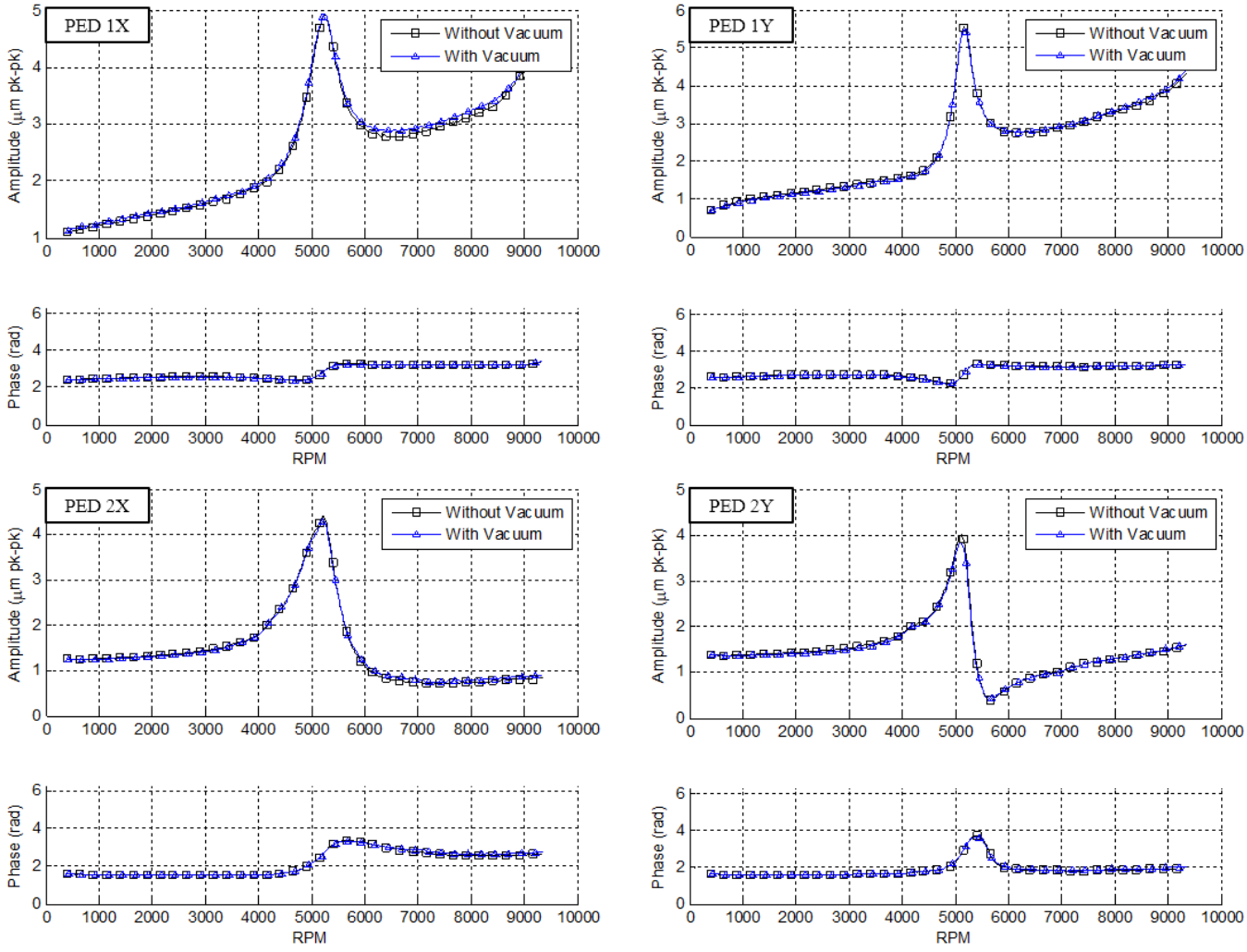

Figure 37: Proximity Probe Measurements for Vacuum and Non-Vacuum Tests

After the initial runs, a 2.8 gram weight was added to balancing holes on the midspan disk. The balancing holes are located at a radius of 127 mm, providing a known unbalance of 356 g-mm or roughly 39,200W/N (SI units). The resulting vibration data from the unbalance

run and base run were vectorially subtracted and compared to predictions, as shown in Figure 38. The predictions include only the vendor pedestal model for simplicity, as all models yield similar results.

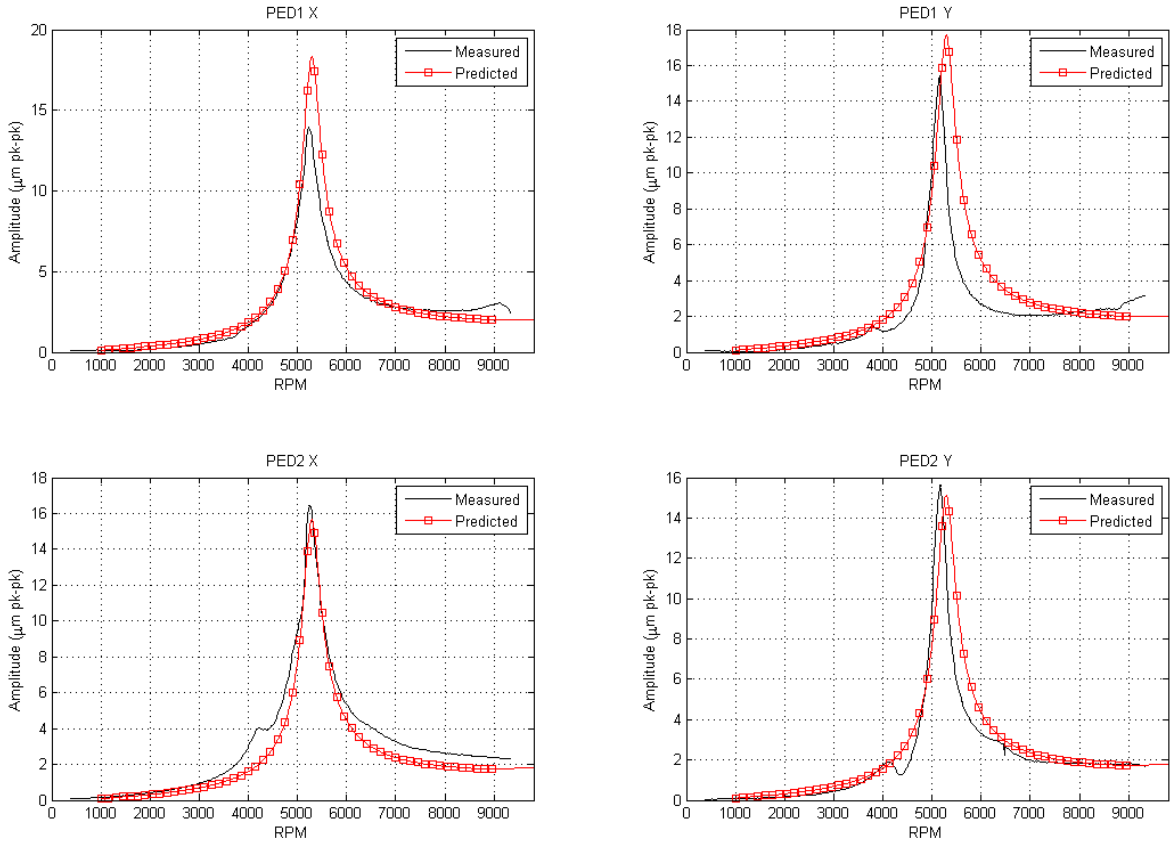

Figure 38: Measurement vs. Prediction for Vacuum Tests

Unlike the previous rotors examined, the measured critical speed locations agreed with predictions within 5% for all probes. In fact, the disagreements seen could easily be attributed to small deviations in bearing clearance measurements, bearing centerline locations during installation, or temperature.

Similar to previous rotors, the pedestal dynamic coefficients were more than 3.5 times the magnitude of the bearing dynamic coefficients, indicating that the pedestals should have little influence in the vibration response. The calculated bearing coefficients for the test rotor with Balancing Facility bearings are provided in *Table 11*.

Table 11: Bearing Coefficients for Test Rotor (Drive End)

Bearing Coefficients (N/μm)					
rpm	Kyy	Kxx	ωCyy	ωCxx	Somm.
1000	36.1	28.5	36.4	31.7	0.0429
2000	52.9	48.5	61.1	58.1	0.8196
3000	73.9	70.6	88.1	86.0	1.2488
4000	96.0	93.0	115.8	114.0	1.6779
5000	118.6	115.8	143.8	142.0	2.1070
6000	141.2	138.5	171.8	170.2	2.5362
7000	163.9	161.3	199.6	197.9	2.9653
8000	187.4	183.9	227.7	225.9	3.3944
9000	210.2	206.7	255.7	255.7	3.8236

The conflicting results between this test and the other unbalance verifications performed may be attributed to one measurement that was not taken previously: the actual bearing centerline locations after rotor installation. Unlike job bearing housings where the bearing locations are known, the bearing locations in the Balancing Facility are set by manually moving each pedestal with a hand crank in an attempt to line up the proximity probes with the burnished areas. This does not lend to high accuracy, and axial deviations of a few centimeters can be expected. Additionally, the proximity probe locations can vary, which means their location in relation to the bearings may be different than the job configuration. These two factors mean that the axial bearing and probe locations in the Balancing Facility may be significantly different than what is modeled for the job rotor.

For reference, the predicted vibration of the test rotor with shorter bearing span is shown in *Figure 39*. By shortening the bearing span by 2.5 cm on each side, the first critical speed is increased by over 8%, and amplitudes are increased significantly.

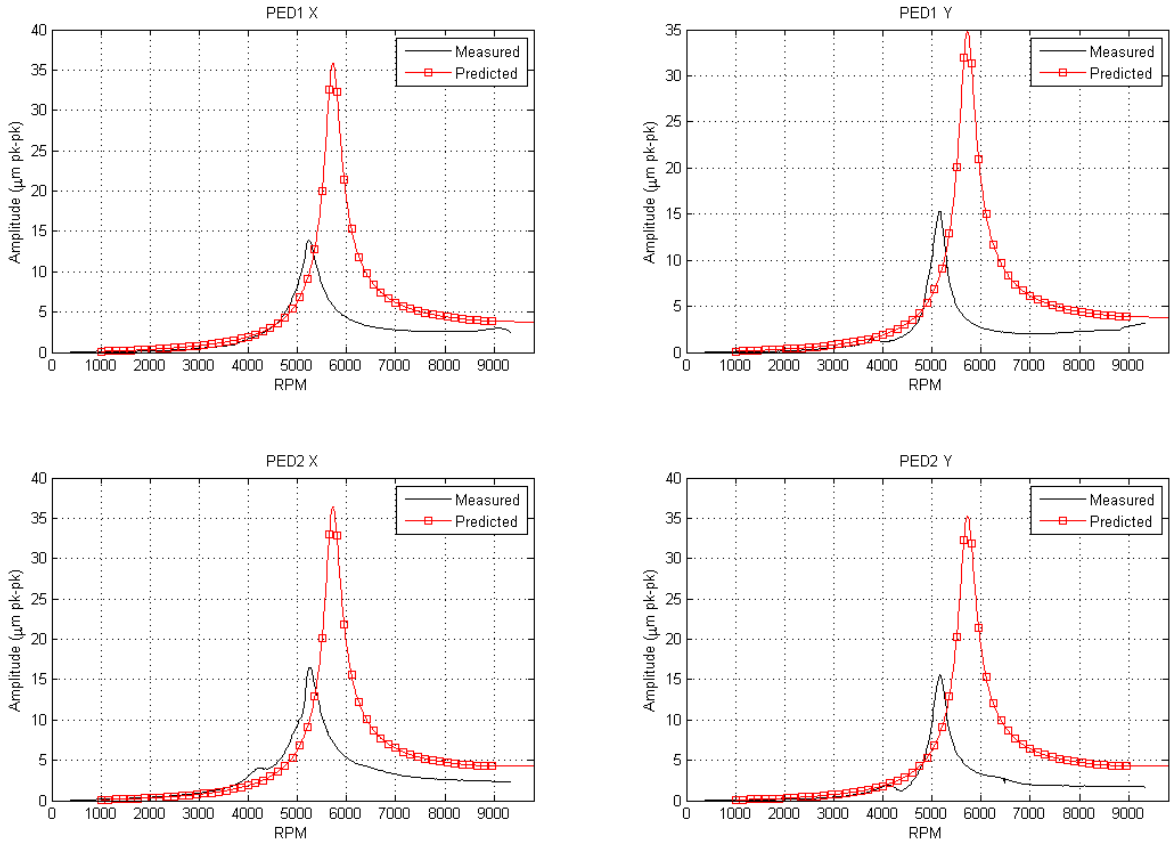

Figure 39: Predicted Test Rotor Vibration with Shorter Bearing Span

The long axial length of the test rotor journal areas permitted the pedestals to be installed in a wide range of axial locations, which prompted the need for bearing centerline measurement. However, it is clear that the bearing centerline locations as installed in the Balancing Facility may be required for all rotors when performing unbalance verifications.

The previously benchmarked rotors can also be examined. Although the actual bearing locations in the Balancing Facility are impossible to know now that the rotors have since been removed, the rotordynamic models can be modified to move the bearing locations. For the 46MB compressor balanced in the DH7 pedestals, moving the bearings outboard as much as possible results in agreement within 5% between the predicted and measured critical speed as shown in Figure 40.

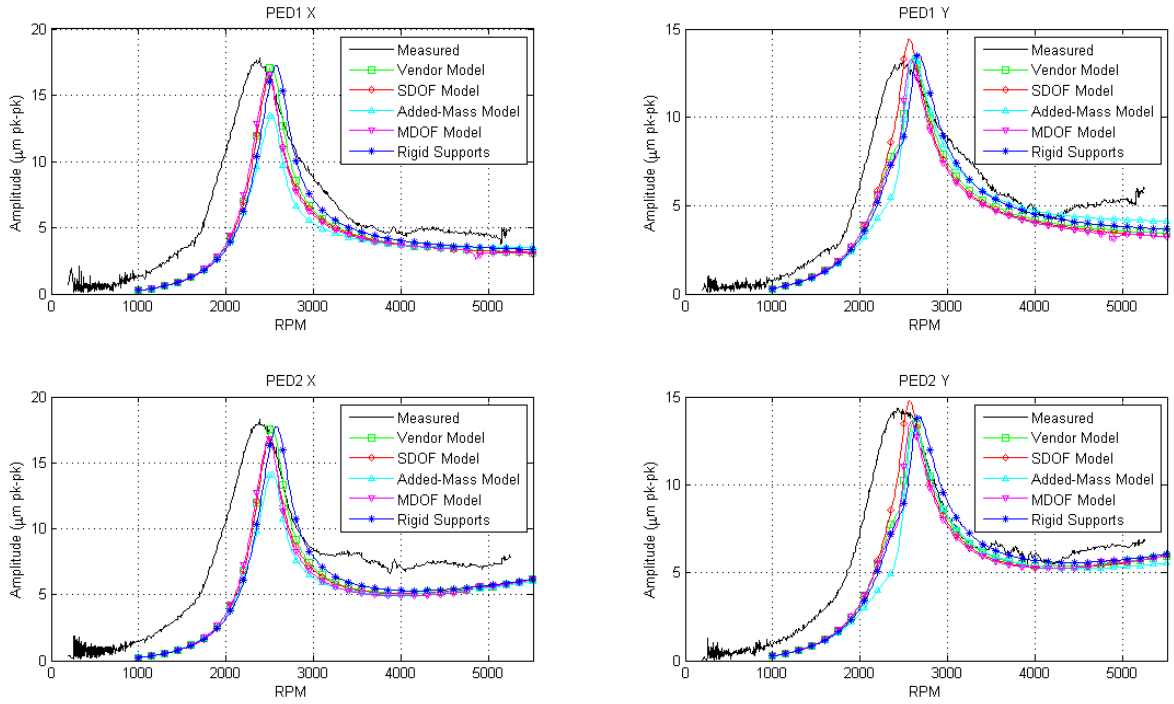

Figure 40: DH7 Benchmark Case with Bearings Shifted Outboard in Model

Additionally, performing a similar analysis on the rotor examined in the DH4 pedestals shows a similar dramatic result. Shifting the bearings outboard as much as possible in this case result in an excellent agreement between the predicted and measured first critical as seen in Figure 41.

Of course, it is important to note that the actual bearing locations for these two benchmark cases are unknown, since this data was not recorded at the time. However, this exercise proves that the change in bearing locations could be a major factor causing the disagreements seen between measurement and prediction in the Balancing Facility. The bearing locations after installation in a Balancing Facility are typically not provided in resulting balancing reports, but it is clear that this information must be recorded when comparing measurements to predictions, or between separate Balancing Facilities.

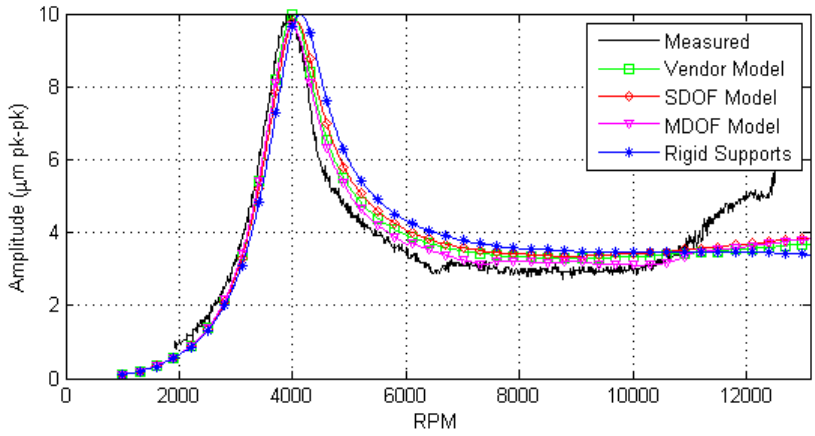

Figure 41: DH4 Benchmark Case with Bearings Shifted Outboard in Model

CONCLUSIONS AND RECOMMENDATIONS

This paper studied the dynamics of the Balancing Facility pedestals.

The API standards related to balancing acceptance criteria were discussed, and relation to the pedestal stiffness was illustrated with data of 723 shop orders.

Extensive modal testing was conducted to all pedestals of the balancing facility in the authors' company. The measured FRFs are curve-fitted, and the parameterized models are compared to those from the Vendor, and those from added-mass (Plug) test. All models were used in the unbalance verification, and the predicted results were presented.

From modal tests and unbalance verification, the following points can be made:

1. All bolts, including bedbolts and bearing cap bolts, should be tightened to proper values to avoid potential problems.

2. All models (the SDOF from measured FRFs, the Vendor model, and the Plug model) yield relatively similar results, which means each of them can be considered a valid method.

3. All models, when used in the analysis, yield similar results in the unbalance verification for the given cases, likely due to the relatively large stiffness of the pedestals (near 3.5 times that of the bearings). Therefore, the authors cannot conclude any one model to be best for the cases examined, even though the MDOF model should be more accurate. Note that the Vendor intentionally tunes the pedestal to move the resonance beyond the operating range. Therefore, as long as the pedestal stiffness is greater than 3.5 times the bearing stiffness, all models are practically equivalent.

4. The relative vacuum conditions in the Balancing Facility have no discernable impact on the bearing dynamics and rotordynamic performance. Tests with and without vacuum conditions yielded nearly identical vibration plots for the case tested.

5. The relative inaccuracy inherent with rotor installation in a Balancing Facility can result in varying bearing spans and probe locations, which must be recorded and reflected in the rotor model.

NOMENCLATURE

Consultant = Outside consulting firm used to measure pedestal dynamics
FRF = Frequency response function
MCS = Maximum continuous speed
MDOF = Multiple degree of freedom
SDOF = Single degree of freedom
Vendor = Original pedestal manufacturer

APPENDIX A: ADDED-MASS METHOD

This method is straight forward based on a single-mass system. As shown in Equations (4), the natural frequency of the system can be calculated based on stiffness and mass.

$$\omega_0 = \sqrt{\frac{kg}{m_0}} \tag{4}$$

When a known mass is added to the original mass, the calculation becomes:

$$\omega_1 = \sqrt{\frac{kg}{m_0 + m_1}} \tag{5}$$

where

ω is natural frequency in rad/s
k is the stiffness in N/m

m is the mass in kg
g is the gravity constant = 9.81 m/s^2

Solving these two equations yields the stiffness and mass:

$$k = \frac{m_1}{g}\frac{\omega_0^2\omega_1^2}{\omega_0^2 - \omega_1^2} \tag{6}$$

and

$$m_0 = m_1\frac{\omega_1^2}{\omega_0^2 - \omega_1^2} \tag{7}$$

The damping can be calculated based on the amplification factor measured from the FRF (see e.g. Ewins, 1984 for details).

$$c = \frac{\sqrt{mk/g}}{AF} \tag{8}$$

where
c is damping in N.s/m
AF is amplification factor
m, k and g are the same as above

APPENDIX B: PEDESTAL TRANSFER FUNCTIONS

The response to a given force input at the pedestals is defined as:

$$\begin{Bmatrix} x \\ y \end{Bmatrix} = \begin{bmatrix} dc_{xx} & dc_{xy} \\ dc_{yx} & dc_{yy} \end{bmatrix}\begin{Bmatrix} f_x \\ f_y \end{Bmatrix} \tag{9}$$

where
x, y are the responses in the x and y directions, respectively.
dc_{ij} is the dynamic compliance measured in the i direction to a force in the j direction
f_x, f_y are the force inputs in the x and y directions, respectively.

The dynamic compliance is measured directly by modal tests. Each term in the dynamic compliance matrix refers to a single frequency response function (FRF). The FRFs are used to calculate polynomial transfer functions.

The transfer function matrix, G(s), for a pedestal is introduced:

$$\begin{Bmatrix} x \\ y \end{Bmatrix} = \begin{bmatrix} g_{xx} & g_{xy} \\ g_{yx} & g_{yy} \end{bmatrix}\begin{Bmatrix} f_x \\ f_y \end{Bmatrix} \tag{10}$$

The components of the transfer function matrix are a function of the complex frequencies. The transfer function matrix was obtained in multiple ways described below.

For a SDOF system, the dynamic compliance for an FRF is defined as:

$$g_{ij}(s) = \frac{1}{-\omega^2 m_{ij} + c_{ij}s + k_{ij}} \tag{11}$$

where
g_{ij} is the transfer function matrix element corresponding to dcij.
ω is the frequency ($\frac{rad}{s}$).
m is the modal mass.
c is the damping.
k is the static stiffness.

For a MDOF system, the transfer function matrix elements are defined as a function of rational fraction polynomials:

$$g_{ij}(s) = \frac{a_n s^n + a_{n-1}s^{n-1} + \cdots + a_1 s + a_0}{b_m s^m + b_{m-1}s^{m-1} + \cdots + b_1 s + b_0} \qquad m > n \tag{12}$$

Where
n is the order of the numerator polynomial.
a_n through a_0 are the numerator polynomial coefficients.

m is the order of the denominator polynomial.
b_m through b_0 are the denominator polynomial coefficients.

Each measurement direction for each pedestal was curve fit using the rational fractional polynomial method (Richardson, 1982) to compute the MDOF transfer function matrices. In this method, s is the normalized complex frequency to an arbitrary frequency limit. In all curve-fits performed in this report, s is normalized against a frequency limit of 400 Hz.

The dynamic stiffness for a pedestal is then defined as the inverse of the transfer function matrix as:

$$[K(s)] = [G(s)]^{-1} \quad (13)$$

An example of the calculated MDOF transfer function (using English units) for the DH7 pedestal 2, stiffening off, horizontal (XX) FRF is provided below.

Table 12. MDOF Transfer Function Polynomial Coefficients Example

Numerator Coefficients (A)		Denominator Coefficients (B)	
a_{19}	-6.6401E03	b_{20}	5.8805E10
a_{18}	2.8124E03	b_{19}	6.7265E10
a_{17}	-2.1288E04	b_{18}	3.0677E11
a_{16}	1.7360E04	b_{17}	2.8928E11
a_{15}	-2.2822E04	b_{16}	6.6629E11
a_{14}	3.9785E04	b_{15}	5.2264E11
a_{13}	-4.2080E03	b_{14}	7.8684E11
a_{12}	4.5754E04	b_{13}	5.1593E11
a_{11}	1.0167E04	b_{12}	5.5245E11
a_{10}	2.9003E04	b_{11}	3.0318E11
a_9	8.8102E03	b_{10}	2.3656E11
a_8	1.0243E04	b_9	1.0834E11
a_7	3.0771E03	b_8	6.0868E10
a_6	1.9129E03	b_7	2.3049E10
a_5	5.0455E02	b_6	8.8918E09
a_4	1.6537E02	b_5	2.7216E09
a_3	3.4656E01	b_4	6.4963E08
a_2	4.9161E00	b_3	1.5212E08
a_1	6.8013E-01	b_2	1.7515E07
a_0	2.7103E-03	b_1	2.7012E06
		b_0	1.0067E04

REFERENCES

API 611, 2008, Reaffirmed 2014, “General-Purpose Steam Turbines for Petroleum, Chemical, and Gas Industry Services”, Fifth Edition, American Petroleum Institute, Washington, D.C.

API 612, 2005, “Petroleum, Petrochemical and Natural Gas Industry – Steam Turbines – Special-purpose Applications”, Sixth Edition,

American Petroleum Institute, Washington, D.C.

API 612, 2014, "Petroleum, Petrochemical and Natural Gas Industry – Steam Turbines – Special-purpose Applications", Seventh Edition, American Petroleum Institute, Washington, D.C.

API 616, 2011, "Gas Turbines for the Petroleum, Chemical and Gas Industry Services", Fifth Edition, American Petroleum Institute, Washington, D.C.

API 617, 2002, "Axial and Centrifugal Compressors and Expander-compressors for Petroleum, Chemical, and Gas Service Industries", Seventh Edition, American Petroleum Institute, Washington, D.C.

API 617, 2014, "Axial and Centrifugal Compressors and Expander-compressors", Eighth Edition, American Petroleum Institute, Washington, D.C.

API 684, 2005, Reaffirmed 2010, "API Standard Paragraphs Rotordynamic Tutorial: Lateral Critical Speeds, Unbalance Response, Stability, Train Torsionals and Rotor Balancing", Second Edition, American Petroleum Institute, Washington, D.C.

API 687, 2001, Reaffirmed 2009, "Rotor Repair", First Edition, American Petroleum Institute, Washington, D.C.

Ewins, 1984, D.J. *Modal Testing: Theory Practice and Application*, Second edition, Research Studies Pr Ltd

ISO 1940-1, 2003, "Mechanical vibration – Balance quality requirements for rotors in a constant (rigid) state – Part 1: Specification and verification of balance tolerances", Second edition, Switzerland

ISO 5343, 1983, "Criteria for evaluating flexible rotor balance", First edition, Switzerland

ISO 11342, 1998, "Mechanical vibration – Methods and criteria for the mechanical balancing of flexible rotors", Second edition, Switzerland

Jackson, C., 1979, *The Practical Vibration Primer*, Gulf Publishing Co., Houston TX.

Nicholas, J. C., Whalen, J. K., and Franklin, S. D., 1986, "Improving Critical Speed Calculations Using Flexible Bearing Support FRF Compliance Data," Proceedings of the Fifteenth Turbomachinery Symposium, Turbomachinery Laboratory, Texas A&M University, College Station, Texas, pp. 69-78.

Nicholas, J. C., Stephen, L. E., Kocur, J.A. and Hustak, J. F., 1997, "Subtracting Residual Unbalance for Improved Test Stand Vibration Correlation," Proceedings of the Twenty Sixth Turbomachinery Symposium, Turbomachinery Laboratory, Texas A&M University, College Station, Texas, pp. 7-18.

Richardson, M. H. and Formenti, D. L., 1982, "Parameter Estimation from Frequency Response Measurements Using Rational Fraction Polynomials", 1st IMAC Conference, Orlando FL, pp 4-10.

Stephenson, RW and Rouch, KE, 1992, *Generating Matrices of the Foundation Structure of a Rotor System from Test Data*, Journal of Sound and Vibration, Volume 154, Issue 3, Pages 467-484

Vazquez, J. A., Barrett, L.E. and Flack, R.D., 2001, "Including the Effects of Flexible Bearing Supports in Rotating Machinery", International Journal of Rotating Machinery, Vol. 7, No. 4, pp. 223-236.

Zhou, S., Sun, Z. and Li, H., 2013, "Dynamic Stiffness Analysis and Modal Identification on Bearing Support of Large-Scale High-Speed Dynamic Balancing Machine", Advances in Vibration Engineering, Vol. 12, No. 6, pp. 587-609.

ACKNOWLEDGEMENTS

The authors would like to thank Elliott Group for permission to publish this paper. In addition, we wish to thank BRG Machinery Consulting for the initial modal testing work reported within this paper.